TREBALL DE FI DE CARRERA

TÍTOL DEL TFC : Aerodynamics, stability and control computational analysis for UAVs

TITULACIÓ: Enginyeria Tècnica Aeronàutica, especialitat Aeronavegació

AUTORS: Carlos Pérez Arroyo
Pol Sintes Arroyo

DIRECTOR: Xavier Prats i Menéndez
Josep Ignasi Rojas

DATA: 24 de juliol de 2007

Títol : Aerodynamics, stability and control computational analysis for UAVs

Autors: Carlos Pérez Arroyo
Pol Sintes Arroyo

Director: Xavier Prats i Menéndez
Josep Ignasi Rojas

Data: 24 de juliol de 2007

Resum

L'objectiu d'aquest projecte és l'estudi aerodinàmic d'un UAV (vehicle aeri no tripulat). Aquest tipus de aeronaus són utilitzades comunament en molts països per desenvolupar tasques com vigilància, recerca o combat degut a la seva autonomia de vol; un UAV pot volar sense un pilot a bord i gràcies a això, pot realitzar tasques molt perilloses sense cap risc.

Els UAVs analitzats en aquest projecte són el Megastar i el Shadow, els quals pertanyen a la EPSC i són utilitzats pel grup Icarus.

L'objectiu d'estudi es la obtenció dels coeficients aerodinàmics de les dos aeronaus per així completar l'estudi de les equacions d'estabilitat i control necessaris per calibrar la programació del pilot automàtic. Per obtenir aquests coeficients s'han utilitzat dos programes diferents: Fluent i Datcom. Fluent es un programa de dinamica computacional de fluids i el Datcom es un programa que et calcula els coeficients aerodinàmics d'una aeronau. La necessitat d'utilitzar ambdós programes recau en assegurar-nos al màxim d'obtenir tots els paràmetres necessaris i per poder validar els resultats comparant-los entre ells.

Les mesures de les geometries i el seu modelatge en el programa de disseny han sigut els passos previs a la simulació de les aeronaus. En aquest punt, han estat simulats en moltes situacions diferents com diferent angles d'atac per així tenir els valors més realistes com es pugui.

Els resultats obtinguts mostren similituds prou significants entre els dos programes en els coeficients aerodinàmics bàsics. L'aspecte on difereixen més es l'angle d'atac crític, però això pot ser degut a la diferència entre com s'introdueixen els paràmetres d'entrada entre els dos programes.

D'aquesta manera, els resultats mostren que Fluent deuria ser utilitzat per calcular paràmetres físics com velocitat o pressió i pels coeficients bàsics (Cl i Cd), gràcies a la seva simulació més real.

Per contra, Datcom pot ser utilitzat com una aproximació per conèixer un munt de coeficients aerodinàmics gràcies als seus ràpids càlculs i a la seva no perfecta entrada de dades de la geometria.

Title : Aerodynamics, stability and control computational analysis for UAVs

Authors: Carlos Pérez Arroyo
Pol Sintes Arroyo

Director: Xavier Prats i Menéndez
Josep Ignasi Rojas

Date: July 24, 2007

Overview

The aim of this Project is the aerodynamic study of an UAV (unmanned aerial vehicle). These types of aircrafts are commonly used in many countries to develop tasks such as surveillance, research or combat due to its autonomy of flight. An UAV can fly without a pilot onboard and contsequently it can realize tasks very dangerous with no risk. The UAVs used in this project are the Megastar and the Shadow, which belong to the EPSC and are used by the Icarus Group.

The objective of this work has been the computation of the aerodynamic coefficients corresponding to two aircrafts in order to calibrate the equations of stability and control needed for the programming of their autopilot. To obtain these coefficients, two softwares have mainly been used: Fluent and Datcom. Fluent is a software based on computational fluid dynamics and Datcom is a program which calculates the aerodynamic coefficients of an specific aircraft. The necessity to use both of them relays in the confidence to obtain as much coefficients as possible and also in the validation of the results comparing the values obtained with both softwares.

The measurements of the geometries and their modelling into a software of design have been the previous steps to the simulation of the aircrafts. At this point, they have been simulated in many situations such as diverse angles of attack to take the more realistic values as possibly.

The results obtained show significant similarities between the two softwares in the basic aerodynamic coefficients. The aspect which they differ more is the critical angle of attack, but this could be because the differences in the way of introducing the parameters between the softwares. In this manner, the results showed that Fluent should be used more for calculate physical parameters such as velocity or pressure and for the basic coefficients (Cl and Cd), thanks to its more realistic calculations. In contrast, Datcom could be used as an approximation to know a lot of aerodynamic coefficients due to its fast calculations and to its approximate geometry inputs.

CONTENTS

LIST OF FIGURES

LIST OF TABLES

INTRODUCTION

Nowadays, new technologies are being developed in order to gain security and effectiveness. Since humans began to think by themselves, the need of knowing what happens all around them and the efforts trying to live longer have been the predominant feelings of all the civilizations. In this way, the UAV were created to free human pilots from several personal risks and to do different tasks that were unable to be done after this technology came to life.

The aim of this Project is the aerodynamic study of an UAV (Unmanned Aerial Vehicle). An UAV could look like a remote controlled aircraft to many people but they have substantial differences between them. An UAV can fly without being controlled by anybody although it needs some orders to know what it has to do. It can roll, yaw or pitch by itself and due to it, it can realize tasks that no controlled aircrafts (radio or human controlled) can do, already be for the risk of the mission or because it cannot be controlled from the distance. UAVs are commonly used in many applications although they were first developed for military tasks. The advantage of these vehicles relays in their capacity to accomplish personnel risk missions and due to it, they are used in fire detecting, rescue or combat missions.

However, to develop an UAV, is needed an autopilot that controls every movement of the vehicle. It could seem very simple at first but the complexity of the equations of stability and control make necessary a complete knowledge of the aircraft parameters. The aircraft has a complete collection of sensors all around which take care of every movement of it but to correct this movements and to control the aircraft itself it is essential to know all the aerodynamic coefficients in order to solve the stability and control equations. Is for this reason that an aerodynamic study is necessary; to obtain the aerodynamic coefficients of stability and control.

In this project, two UAVs are studied and modelled in order to get these coefficients. The steps to obtain them are the modelling of the geometries in a computer design program and the simulation in aerodynamic softwares. To obtain all the coefficients as possible and to get the more realistic values, two softwares are used: Fluent and Datcom. Fluent is a CFD (Computational Fluid Dynamics) software from which are obtained the basic lift and drag coefficients and other parameters such as pressure, velocity or temperature. Datcom, is a software from the U.S. Air Force that calculates the stability and control equations from an approximately aircraft geometry and from it, much more coefficients (including the lift and the drag coefficients) are obtained.

The project is structured in six chapters. The first three chapters are an introduction to the basic concepts of UAVs, stability and control, aerodynamics and softwares used. The fourth chapter explains some initials CFD simulation and the simulation itself and the chapter five discuss the Datcom inputs and outputs. Finally, in chapter six there is a comparative of the common results obtained from Fluent and Datcom.

CHAPTER 1. UNMANNED AERIAL VEHICLES

1.1. Introduction to UAVs

An Unmanned Aerial Vehicle (UAV)[1] is an aircraft with no onboard pilot. It was first created by the military of the United States during the First World War. It was no more than a radio controlled airplane that was used to carry missiles but it was the first step for the development of this technology. They soon realize the effectiveness in military applications such as surveillance, bombing and ground attacks and they are becoming a great instrument in civil tasks like search and rescue.

The UAV itself looks like a radio controlled aircraft but it has the capability of being autonomous during the flight. So the main difference is the autonomy of the vehicle; in the radio controlled aircrafts, an operator, is the one who controls it and give orders of what to do in every moment of the flight but in the other side, with the UAV, is the vehicle itself who knows what to do thanks to an automatic pilot that control every system of the aircraft.

However, the UAV have different qualities between them. There are more autonomous vehicles than others and some of them can fly more time than the rest but as it has been said before, all the UAV are autonomous and do not have a pilot onboard.

Finally, it should be remarked that in these days the term UAS (Unmanned Aircraft System) is commonly being used. The initials include the UAV, their systems and all the equipment necessary to flight the vehicle and to manage the information about the task it is doing.

1.1.1. UAV Classification

Many different criteria for UAV classification have been proposed. There are classifications that follow the final application of the vehicle and there are others which follow the characteristics of each UAV, specially their operational range.

In the classification of the United States [2] showed in Fig. 1.1, the UAV are divided into two big groups; tactical UAVs (TUAVs) are defined as those having a maximum operational range of 200 km and mostly intended for direct support of ground forces, and Endurance UAVs are the ones that have an operational range beyond 200 km. TUAVs include short range (less than 50 km range) and medium range types. Endurance models are further sub-divided into Medium and High Altitude (Long) Endurance (MALE and HALE) vehicles with endurance on 10-30 hours and more than a day respectively. Notional future Ultra Long Endurance (ULE) UAVs may be able to stay aloft for months.

The final application classification can be divided into two categories: the civil and the military. Probably, it could be a third category, but in many cases is grouped in one of the two main categories. This would be the research and development group.

In the military group, we can find lots of different types of UAV. It can be divided into three categories. These are:

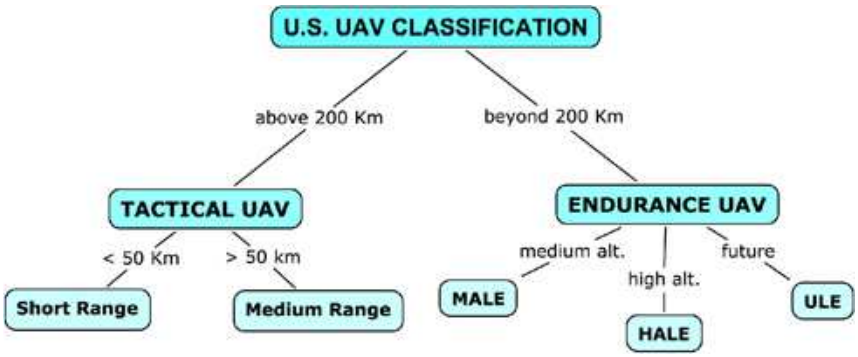

Figure 1.1: United States UAV Classification. Source: [2]

- Target and Decoy
- Reconnaissance
- Combat

The military industry, as in many cases, is the one that has start the development of such technology and leads today the UAV industry. In the civil group, there is not a possible classification because the civil UAVs can have a great range of applications but the suitability of UAVs in dangerous missions, the increasing success of UAVs in service and demonstration, or the increases in payload capability has lead to many technology publications to cite a wide range of applications that include UAVs taking on new missions, replacing the methods for existing missions and adding a new dimension to existing missions. Examples of these missions include:

- Border & Costal Patrol and Monitoring
- Homeland Security
- Law Enforcement & Disaster Operations
- Digital Mapping & Planning/Land Management
- Search & Rescue
- Fire Detection and Fire Fighting Management
- Communications and Broadcast Services
- Precision Agriculture and Fisheries
- Ground Transportation Monitoring and Control
- Satellite Augmentation Systems
- Air Traffic Control Support
- Power Transmission line Monitoring

- Environmental Research & Air Quality Management/Control

In order to have an idea of what can do this class of vehicles and what characteristics do they have, there is an explanation of some important UAVs in Appendix. A.

There are a lot of different models all over the world but the most important are the ones above commented.

1.2. ICARUS Group

The UAVs analyzed in this project, are the UAV belonging to the Icarus [3] Group of the Technical University of Catalonia (UPC).

The ICARUS research group is composed by researchers from the Computer Architecture Department of the Technical University of Catalonia and belongs to the Aeronautic and Aerospace Research Group (CRAE) of the UPC. The research of the ICARUS group is focused in the topic of Unmanned Aerial Vehicles (UAV). The targets of the research are technologies that allow to build low cost UAVs and to manage then for several civil missions as far as autonomous as they could be [4].

The two vehicles studied in this work are the Shadow and the Megastar, two of the three models in possession of this group.

The Shadow UAV is a Pakistani model from 'Integrated Dynamics' [5]. This company has the Shadow UAV Series and the one acquired by the Icarus Group is the Shadow mk-1.

The other vehicle is a radio controlled model smaller than the Shadow that has been transformed into an UAV with the same function of the Shadow: preventing and detecting fires. This model is the Megastar and is a predecessor of the Shadow for the group.

CHAPTER 2. BACKGROUND ON AERODYNAMICS, STABILITY AND CONTROL

2.1. Basics of Aerodynamics

2.1.1. Bernoulli's theorem

The Bernoulli's theorem is based on the conservation of energy and continuity principle and it will explain how the aerodynamic forces are generated. A flow which is inviscid, incompressible, steady and one dimensional will be considered in order to explain Bernoulli's theorem.

The energy in the flow is composed of several energies. The kinetic energy arises because of the directed motion of the fluid; the pressure energy is due to the random motion within the fluid; and the potential energies due to the position of the fluid above some reference level. Bernoulli's theorem is an expression of the conservation of the total energy; that is, the sum total of these energies in a fluid flow remains a constant along a streamline. Expressed concisely, the sum of the kinetic energy, pressure energy, and potential energy remains a constant.

The continuity principle is a statement of the conservation of mass in a system. Considering a fluid that flows through a tube with different cross section areas. The continuity equation states that the fluid mass passing section 1 per unit time must equal the fluid mass passing section 2 per unit time. In fact, this mass flow rate must be the same value at any cross section examined in Fig. 2.1 [6]:

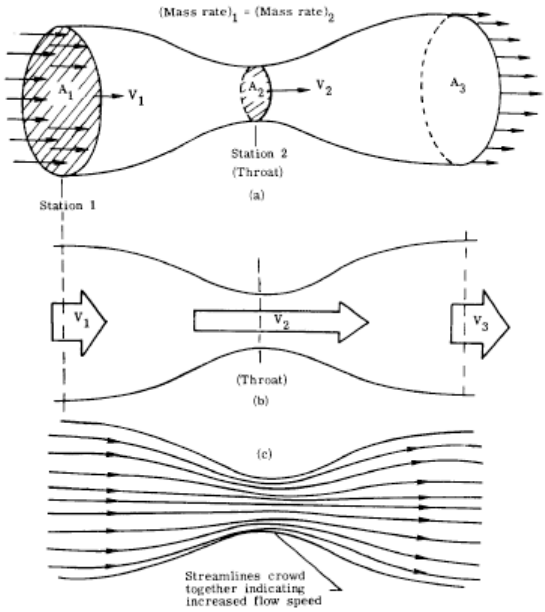

Figure 2.1: Venturi tube and continuity principle. Source: [6]

If it is further assumed that the fluid flow is horizontal (as, for example, airflow approaching an aircraft in level flight), then the potential energy of the flow is a constant. Bernoulli's theorem reduces to Eq. 2.1

$$Kineticenergy + Pressureenergy = Constant \tag{2.1}$$

If energy per unit volume is considered Bernoulli's theorem may be expressed in terms of pressure. The kinetic energy per unit volume is called dynamic pressure q and is determined by ρ and v at the point in question. The pressure energy per unit volume (due to random motion within the fluid) is the static pressure of the fluid and is given the symbol p. The constant energy per unit volume is called the total pressure p_t.

Then, Bernoulli's equation reduces to Eq. 2.2 or Eq. 2.3.

$$Dynamicpressure + Staticpressure = Total pressure \tag{2.2}$$

$$\frac{1}{2}\rho v^2 + p = p_t \tag{2.3}$$

Bernoulli's equation states that in a streamline fluid flow, the greater the speed of the flow, the less the static pressure; and the less the speed of the flow, the greater the static pressure. There exists a simple exchange between the dynamic and the static pressures such that their total remains the same. As one increases, the other must decrease. As the dynamic pressure is referred to v, if the static pressure decreases, the speed has to increase.

The Bernoulli's theorem applied to an airfoil means that, the air increases its speed over the exterior surface of the airfoil (upper surface) decreasing its pressure. Even though, the air decreases its speed over the inferior surface of the airfoil (intrados) increasing its pressure.

The difference of pressures (see Eq. 2.4) applied to the surface origins the aerodynamic force of lift. The difference of pressures and others causes that origins the aerodynamics forces are explained in more detail in section 2.1.2..

$$F = \Delta P \cdot S \tag{2.4}$$

2.1.2. Aerodynamics forces and moments

Force is every cause that changes the state of remain or movement of a body [7]. In an aircraft, there are different forces that exerts on it. Lift and drag are considered aerodynamics forces. The other forces may be weight and thrust.

The aerodynamics forces and moments on the body are due to:

- Pressure distribution over the body surface

- Shear stress distribution over the body surface

As shown in Fig. 2.2, p acts normal to the surface, and τ acts tangential to the surface. Shear stress is due to the ”tugging action” on the surface, which is caused by friction between the body and the air.

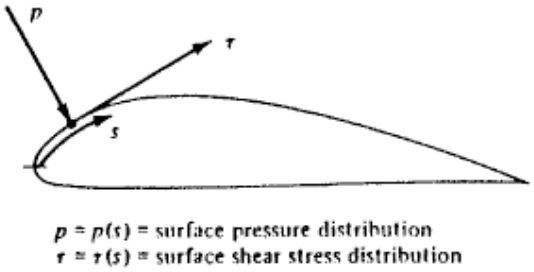

Figure 2.2: Illustration of pressure and shear stress on an aerodynamic surface. Source: [7]

The net effect of the p and τ distributions integrated over the complete body surface is a resultant aerodynamic force R and moment M on the body as shown in Fig. 2.3 where V_∞ is the relative wind, defined as the flow speed far ahead of the body. The flow far away the body is called the free stream, and hence V_∞ is also called the free stream speed.

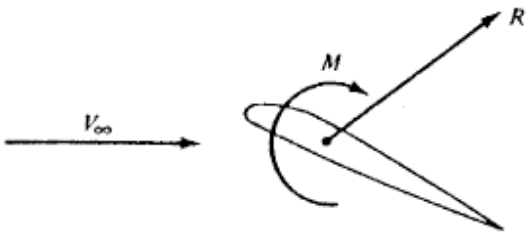

Figure 2.3: Resultant aerodynamic force and moment on the body. Source: [7]

By definition (see Fig. 2.4):

- $L \equiv$ lift $\equiv$ component of Rperpendicular to V_∞
- $D \equiv$ drag $\equiv$ component of R parallel to V_∞
- The chord c is the linear distance from the leading edge to the trailing edge of the body.
- $N \equiv$ normal force $\equiv$ component of R perpendicular to c
- $A \equiv$ axial force $\equiv$ component of R parallel to c
- The angle of attack $\equiv$ aoa $\equiv$ is defined as the angle between c and V_∞.

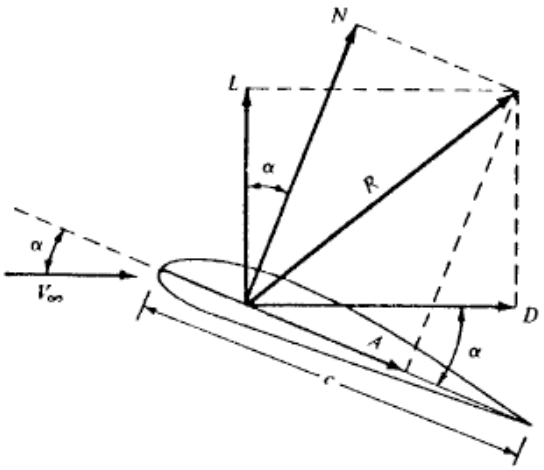

Figure 2.4: Resultant aerodynamic force and the components into which it splits. Source: [7]

It is possible to obtain a geometrical relation of these variables as seen in Eqs. 2.5 and 2.6

$$L = N\cos\alpha - A\sin\alpha \tag{2.5}$$

$$D = N\sin\alpha + A\cos\alpha \tag{2.6}$$

Consider the two-dimensional body sketched in Fig. 2.5. The chord line is drawn horizontally, and hence, the relative wind is inclined relative to the horizontal by the angle of attack α. An arbitrary point A is selected on the upper surface to a distance s_w and similarly, a point B on the lower surface to a distance of s_l, At a given point, the pressure is normal to the surface and is oriented at an angle θ relative to the perpendicular and shear stress is tangential to the surface and is oriented at the same angle θ relative to the horizontal. The sign convention for θ is positive when measured clockwise.

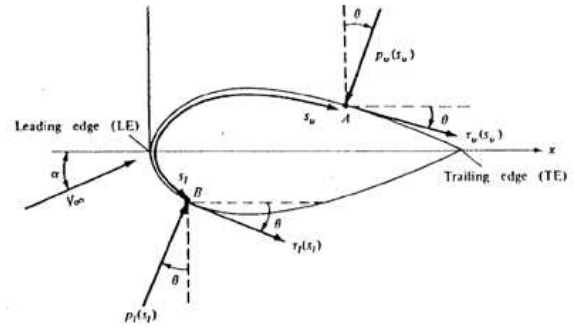

Figure 2.5: Nomenclature for the integration of pressure and shear stress distributions over a two-dimensional body surface. Source: [7]

Now consider Fig. 2.5 as a cross section of an infinitely long cylinder of uniform section as shown in Fig. 2.6. If an elemental surface area dS is considered, the total normal force N' and the total axial force A' are generated due to the pressure and shear stress on the elemental area dS. The primes denote foce per unit span and they are represented by

Eqs. 2.7 and 2.8 and their respectives for the lower surface (denoted by the sub index l) Eq. 2.9 and 2.10.

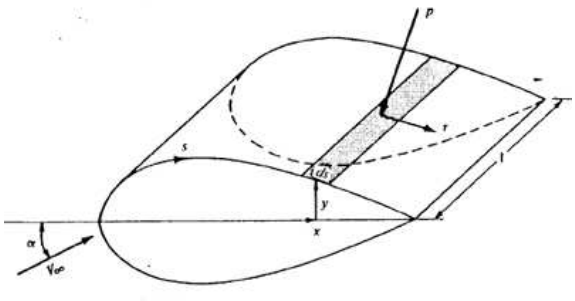

Figure 2.6: Aerodynamic force on an element of the body surface. Source: [7]

$$dN'_u = -p_u ds_u \cos\theta - \tau_u ds_u \sin\theta \tag{2.7}$$

$$dA'_u = -p_u ds_u \sin\theta + \tau_u ds_u \cos\theta \tag{2.8}$$

$$dN'_l = -p_l ds_l \cos\theta - \tau_l ds_l \sin\theta \tag{2.9}$$

$$dA'_l = -p_l ds_l \sin\theta + \tau_l ds_l \cos\theta \tag{2.10}$$

The total normal and axial forces to the surface are obtained by integrating Eqs. 2.7, 2.8, 2.9, 2.10 in all the edge of the airfoil (Trailing edge and leading edge). The result of the integration is shown in Eqs. 2.11, 2.12 [7].

$$N'_u = -\int_{LE}^{TE} (p_u \cos\theta + \tau_u \sin\theta)\, ds_u + \int_{LE}^{TE} (p_l \cos\theta - \tau_l \sin\theta)\, ds_l \tag{2.11}$$

$$A'_u = \int_{LE}^{TE} (-p_u \sin\theta + \tau_u \cos\theta)\, ds_u + \int_{LE}^{TE} (p_l \sin\theta + \tau_l \cos\theta)\, ds_l \tag{2.12}$$

Momentum equation (Eq. 2.13is obtained in a similar way to the previous one. Momentum is referred to a point, Eq. 2.13 is the moment about the leading edge per unit span.

$$\begin{aligned} M'_{LE} = &\int_{LE}^{TE} [(p_u \cos\theta + \tau_u \sin\theta)\, x - (p_u \sin\theta - \tau_u \cos\theta)\, y]\, ds_u + \\ &+ \int_{LE}^{TE} [(-p_l \cos\theta + \tau_l \sin\theta)\, x + (p_l \sin\theta + \tau_l \cos\theta)\, y]\, ds_l \end{aligned} \tag{2.13}$$

2.1.3. Aerodynamic coefficients

There are some quantities of an even more fundamental nature than the aerodynamic forces and moments themselves called dimensionless force and moment coefficients. The coefficients are referred to S, the reference area and l, the reference length and de dynamic pressure (see Eqs. 2.2 and 2.3). These coefficients are defined in Eqs. 2.14 to 2.18.

$$C_L \equiv \frac{L}{q_\infty S} \tag{2.14}$$

$$C_D \equiv \frac{D}{q_\infty S} \tag{2.15}$$

$$C_N \equiv \frac{N}{q_\infty S} \tag{2.16}$$

$$C_A \equiv \frac{A}{q_\infty S} \tag{2.17}$$

$$C_M \equiv \frac{M}{q_\infty S l} \tag{2.18}$$

The reference area S and reference length l are chosen to pertain to the given geometric body shape and they can be different if there are different shapes. Some reference areas and reference lengths are shown in Fig. 2.7.

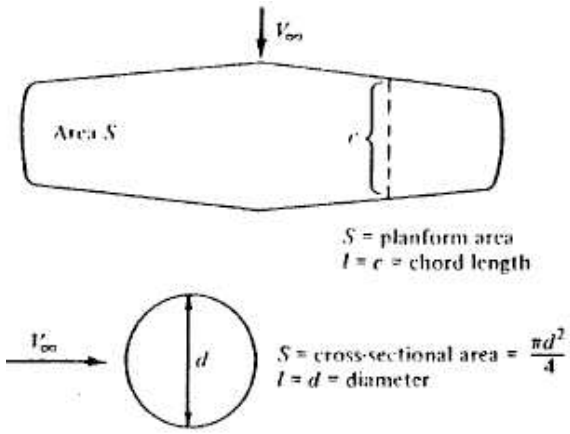

Figure 2.7: Some reference areas and reference lengths. Source: [7]

If the Cl and Cd coefficients are divided a relationship is obtained (see 2.19). The lift-drag ratio is a mesure of the aerodynamic efficiency of the airplane. For a particular airplane the lift-drag ratio varies with the angle of attack of the airplane. There is a maximum angle of attack for which this ratio is a maximum. This is then the angle of attack for minimum glide angle and maximum range.

$$\frac{Cl}{Cd} = \frac{L}{D} = f(\alpha) \tag{2.19}$$

2.2. Control

Control [8] refers to the ability to initiate and sustain changes in angle of attack, slip or bank. An aircraft has three axes:

- Lateral.
- Longitudinal.
- Normal (vertical) or directional

An aircraft can rotate around each of the three axes. The rotating motions and the corresponding axes are (see Fig. 2.8):

- Roll $\equiv$ motion around the longitudinal axe.
- Pitch $\equiv$ motion around the lateral axe.
- Yaw $\equiv$ motion around the directional axe.

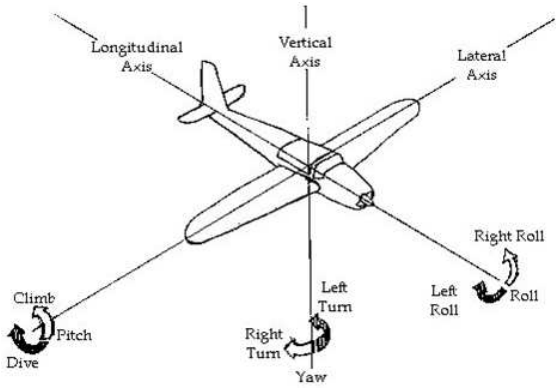

Figure 2.8: Stability axis. Source: [8]

Roll control is provided by the ailerons. When the ailerons are deflected the down going aileron increases the camber of one wing. The up-going aileron decreases camber on the other wing. The result is an asymmetric lift between the wings. These causes the roll rate to increase away from the wing with the greater lift. Directional or yaw control is provided by the rudder. Pitch control is provided by the elevators. A pitch damping effect quickly develops once the elevators are deflected. As a result the aircraft soon establishes a constant pitch rate once the elevators are deflected.

2.3. Stability

Stability [9] refers to how an aircraft responds to changes in angle of attack, slip or bank. It exists static and dynamic stability, which are commented later and it can be categorized as positive, negative or neutral.

Positive stability refers to when once the force is removed, the object moves back toward the starting point. When the force is removed and the object continues to move further away from the starting point, this is negative stability.

Finally, neutral stability occurs when the object stops moving after a force is removed. It has no tendency to return or diverge further.

Static stability refers to the aircraft's initial response when disturbed from a given angle of attack, slip or bank. Opposite, the Dynamic stability refers to the aircraft response over time when disturbed from a given angle of attack, slip or bank.

2.3.1. Directional stability

Static directional stability is a measure of the aircraft's resistance to slipping. The greater the static directional stability the quicker the aircraft will turn into a relative wind which is not aligned with the longitudinal axis. The main contributor to the static directional stability is the fin. Both the size and arm of the fin determine the directional stability of the aircraft. The further the vertical fin is behind the centre of gravity the more static directional stability the aircraft will have.

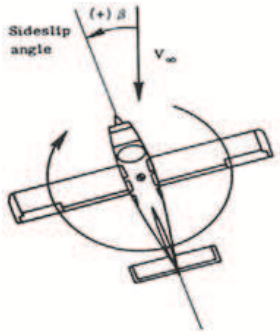

Figure 2.9: Sideslip angle. Source: [8]

2.3.2. Lateral stability

When the aircraft is flying in straight flight (no slip) with the ailerons neutral both wings produce the same amount of lift. This is true because both wings are at the same angle of attack and flying at the same velocity. If the pilot deflects the ailerons then one wing will produce more lift than the other (because it now has more camber.) This causes a rolling moment. The aircraft will begin to roll and will continue to roll, faster and faster, as long as one wing produces more lift than the other. The tendency for the roll rate to become constant is called roll damping. This helps to establish lateral stability but it is not enough.

Dihedral is the most common design feature used to increase the lateral stability. For example, if an aircraft has a bank of some degrees, the lateral component of the lift vector, causes the aircraft to slip to one side. As a result, the relative wind flows across the wings at an angle. Then, the relative wind strikes the upper wing at a smaller angle of attack than

the lower wing so the upper wing produces less lift. Finally, the bank return to 0 and the two wings produce same lift (see Fig. 2.10).

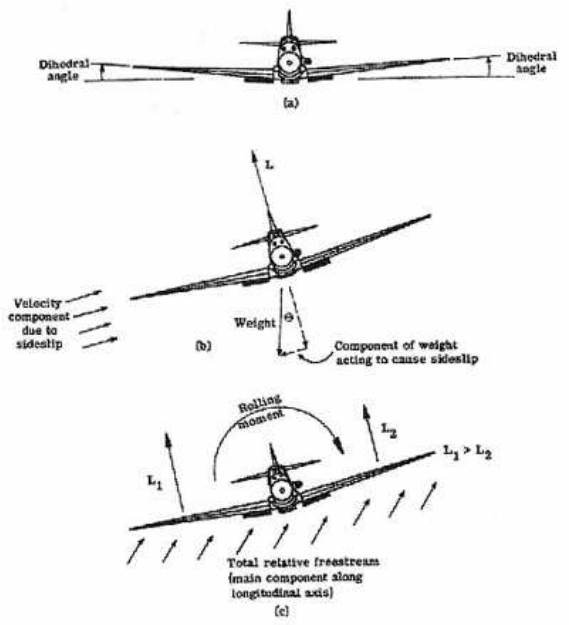

Figure 2.10: Movements of the lateral stability. Source: [8]

Moreover, many aircrafts suffer a dynamic instability problem known as Dutch Roll. Dutch roll happen when the aircraft has relatively strong static lateral stability and weak directional stability. In a Dutch roll the aircraft begins to yaw due to a gust or other input. The yaw is slow damping out so the aircraft begins to roll before the yaw is stopped.

By the time the yaw stops and begins to swing back toward zero slip, the aircraft has developed a considerable roll rate and due to momentum plus the slip angle, the aircraft continues to roll even once the nose has begun returning to the original slip angle.

Eventually the yaw overshoots the zero slip angle causing the wings to begin rolling back in the opposite direction. The whole procedure repeats, sometimes with large motions, sometimes with just a small churning motion. Like all dynamic stability problems, Dutch roll is much worse at high altitudes where the air is less dense.

2.3.3. Longitudinal stability

Longitudinal stability refers to stability around the lateral axis. It is also called pitch stability. It depends on the location of the centre of gravity. This is the most important thing to realize as a pilot.

If the aircraft is loaded within the approved centre of gravity envelope it will have positive static longitudinal stability. That is critical, because an aircraft with negative longitudinal stability would be impossible to fly for more than a few moments. It would require tremendous concentration to avoid overcontrolling such an aircraft.

Most aircraft would be completely unstable without the horizontal stabilizer. The stabilizer

provides the same function in longitudinal stability as the fin does in directional stability. When the angle of attack changes it tends to pitch the aircraft back to its original angle of attack. The main wing, on the other hand, may be stable, or unstable, depending on the exact location of the centre of gravity.

The situation of the centre of gravity with respect of the aerodynamic centre has a lot of influence in the longitudinal stability. The Fig. 2.11 and Fig. 2.12 are examples of positive, negative and neutral longitudinal stabilities respectively.

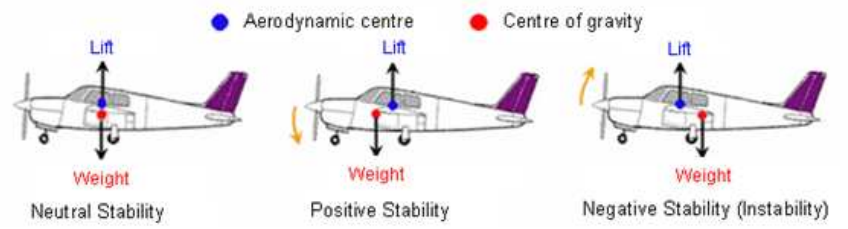

Figure 2.11: Positives, negatives and neutral stabilities. Source: [8]

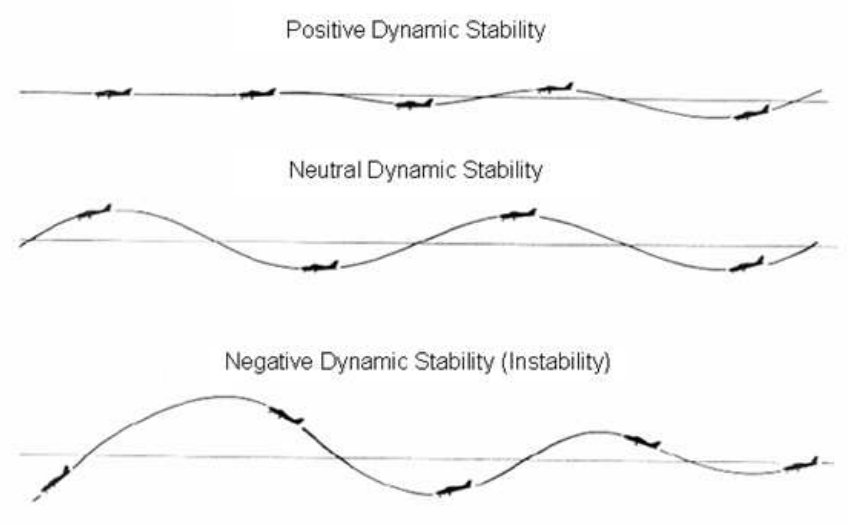

Figure 2.12: Movements of the different stabilities. Source: [8]

2.4. Automatic pilot

An Automatic Pilot or autopilot [10] is a mechanical, electrical, or hydraulic system used to guide a vehicle without assistance from a human being.

The original use of an autopilot was to provide pilot relief during cruise modes. Autopilots now perform functions more rapidly and with greater precision than the human pilot. The functions, designs, and uses of autopilots vary widely depending on the type of vehicle. An autopilot is unique equipment so that it is expected to make the aircraft fly in the

same manner as a highly trained proficient pilot. It must provide smooth control and avoid sudden and erratic behaviour. The intelligence for control must come from sensors such as gyroscopes, accelerometers, altimeters, airspeed indicators, automatic navigators, and various types of radio-controlled data links.

Sophisticated autopilots are no longer limited to military aircraft but are now common in commercial aircraft and are available for general aviation. In modern fly-by-wire aircraft the autopilot and the flight control system often reside together in the same digital computer, and it is difficult to separate their functions. These advanced systems provide the pilot relief functions plus help to stabilize the aircraft, protect the aircraft from undesirable manoeuvres, and provide automatic landings

Aircraft motion is usually sensed by a gyro, which transmits a signal to a computer. The computer commands a control servo to produce aerodynamic forces to remove the sensed motion.

The computer may be a complex digital computer, an analogue computer (electrical or mechanical), or a simple summing amplifier, depending on the complexity of the autopilot. The control servo can be a hydraulically powered actuator or an electromechanical type of surface actuation. Signals can be added to the computer that supplies altitude commands or steering commands (see Fig. 2.13).

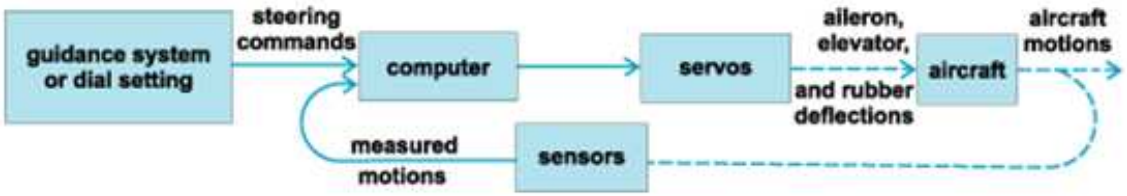

Figure 2.13: Scheme of the autopilot. Source: [10]

Moreover, in order to sense all three axes, there should be a gyro for each exe so that every motion is sensed and controlled.

The specifications of the Shadow UAV autopilot used in the Icarus Group can be found in the annex B.

CHAPTER 3. SOFTWARE USED

This chapter will explain the different software used in this project . Every software used has it own purpose on this project, some of them were used as auxiliar programs an other as a requirement of the project. There are software used to create the geometry, mesh the models, make a CFD simulation, etc. For more information about the aerodynamic softwares used in this work see [11].

3.1. Gambit 2.2.30

Gambit [12] is a software package designed to help analysts and designers build and mesh models for computational fluid dynamics (CFD) and other scientific applications. Gambit receives user input by means of its graphical user interface (GUI). The Gambit GUI makes the basic steps of building, meshing, and assigning zone types to a model simple and intuitive, enough to accommodate a wide range of modeling applications.

A mesh consists in a three-dimensional grid that envelops the model of study. The discrete points of the mesh are used to calculate the flow field values. The mesh tries to discretize the model. Some discrezitation techniques are explained in Appendix. D.2.

Gambit will help us to mesh our models of study. Different meshes for different angles of attack of our models have to be done in order to make a good simulation. A size function will be used to mesh our models in order to mesh it finer near the model. A typical stable growth rate for the size functions is between 1.1 and 1.3. The size function helps us to focus on the walls, where the boundary layer is more affected by the viscosity.

The next step after creating the mesh is choosing the boundary conditions of the entire model. Boundary conditions specify the flow and thermal variables on the boundaries of your physical model. They are, therefore, a critical component of your CFD simulations and it is important that they are specified appropriately.

Our boundary conditions are (see Fig. 3.1):

- VELOCITY_INLET: This boundary condition permits us to input the velocity of the free air stream of our simulations.
- PRESSURE_OUTLET: Pressure outlet boundary conditions require the specification of a static pressure at the outlet boundary. It is selected at the outlet of the computational wind tunel.
- WALL: Wall boundary conditions are used to bound fluid and solid regions. The walls of the computational wind tunel and the walls of the models are defined as WALL.
- SYMMETRY: Symmetry boundary conditions are used when the physical geometry of interest, and the expected pattern of the flow/thermal solution, have mirror symmetry. As our three-dimensional models are symmetric, SYMMETRY is very useful to spare time calculation because the simulation is only run on the half of the model.

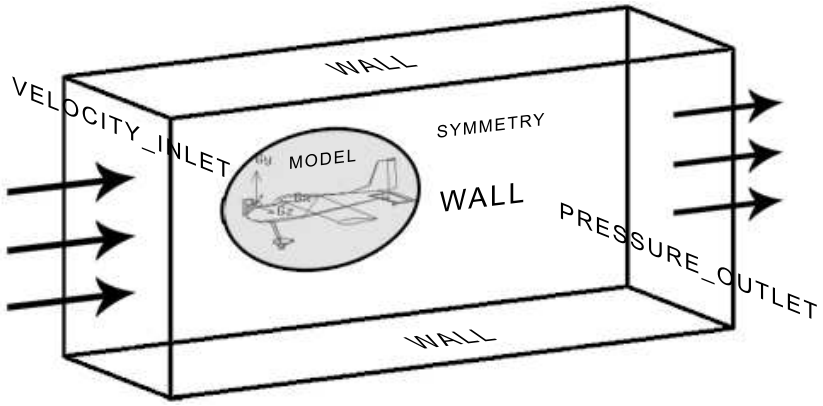

Figure 3.1: Boundary conditions

3.2. Fluent 6.2.16

Fluent [13] is a CFD (Computational Fluid Dynamics) computer program for modeling fluid flow and heat transfer in complex geometries. Fluent provides complete mesh flexibility, including the ability to solve your flow problems using unstructured meshes that can be generated about complex geometries.

The CFD programs as Fluent solve the different governing equations of motion(see C), heat transfer, etc. In order to accomplish this task Fluent needs to import a mesh to make the simulation. The equations will be solved in the points contained in the mesh.

Fluent permits to enter the values of the different boundary conditions as the velocity at the VELOCITY_INLET, the materials used in our geometry or the pressure of the volume. Most of the input parameters will be left with the default values. The default values are the sea level standard parameters.

Before starting the simulation the solver has to be choosen. Some difference of the solvers are explained in Appendix. D. The next step is to choose the viscous model. Once initialized the initial parameters as velocity or pressure the iteration can be started.

After a few iterations (the number of iterations depends on the simulation and the convergence parameters) the results of our simulations are obtained. The results of interest for our project are the force reports. The force reports permit to obtain the coefficients of lift and drag. As seen on Section. 2.1.3. these values have to be referred to an specific area or length, a velocity and other values as viscosity or temperature.

3.3. Datcom

Datcom ([14] and [15]) is a FORTRAN language program designed by the USAF (U.S. Air Force) to minimize the human and time costs that existed in the calculations of the large and complex equations of stability and control of the aircrafts. In this way, USAF

Digital Datcom, is an approach to provide rapid and economical estimation of aerodynamic stability and control characteristics.

Moreover, this is very useful software in order that it makes able to calculate different aerodynamic characteristics of an aircraft that in not yet produced. The advantages are very significant so these characteristics can be applied to a generic flight simulation program, consequently yielding a representative simulation of the aircraft.

The program itself is based in an input file that contains all the characteristics of the aircraft needed to obtain the different coefficients. This file is a .dcm file and is composed by a series of namelist statements listing input variables which describe the aircraft under consideration and variables which control the execution and output of the software. The input file is divided into four sections:

- Flight conditions and reference dimensions
- Basic configuration geometry
- Additional configuration definition
- Control of the execution and user specifications

However, the complexity of the software relays in the outputs files created. Newest versions of Datcom have more friendship interaction due to new plotting and visualization utilities. The software creates four input files (as shown in Fig. 3.2). The original files were an .out and a .lfi ones that plotted all the coefficients in the screen. This new version also has a .ac file that permits the visualization of the geometry you have describe in the input file and .png files that you can open in programs like Photoshop that contains all the coefficient graphics of the airplane under consideration.

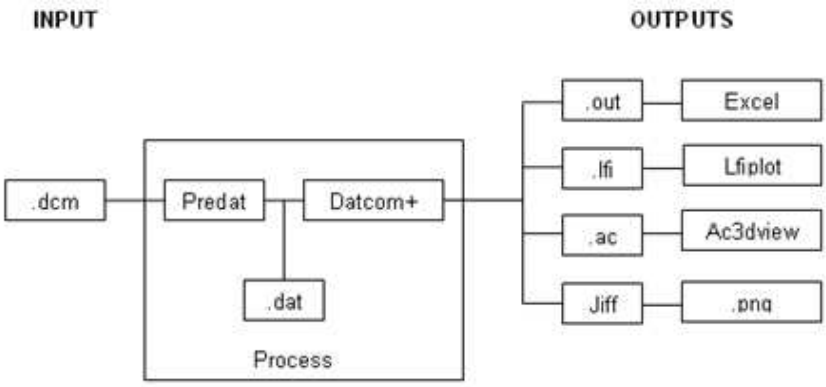

Figure 3.2: Datcom software running. Source: [14]

3.4. PABLO

PABLO (see [16]) is the acronym of Potential flow around Airfoils with Boundary Layer coupled One-way and it is a pedagogical low-speed airfoil analysis program written in

MATLAB. It uses a one way coupled inviscid + boundary layer model.

The inviscid flow is solved using a Panel Method. The boundary layer equations use the inviscid flow velocity provided by the panel method, but the effect of the boundary layer on the inviscid flow is not taken into account.

PABLO is used in section 4.1. to help us to determine the Cl and Cd coefficients for a specific airfoil.

3.5. XFOIL 6.96

XFOIL (see [17]) is an interactive program for the design and analysis of subsonic isolated airfoils. It consists of a collection of menu-driven routines which perform various useful functions such as:

- Viscous (or inviscid) analysis of an existing airfoil.
- Airfoil design and redesign by interactive specification of a surface speed distribution via screen cursor or mouse.
- Airfoil redesign by interactive specification of new geometric parameters.
- Blending of airfoils.
- Drag polar calculation with fixed or varying Reynolds and/or Mach numbers.
- Writing and reading of airfoil geometry and polar save files.
- Plotting of geometry, pressure distributions, and polars.

The source code of XFOIL is Fortran 77. The plot library also uses a few C routines for the X-Windows interface.

XFOIL is used in section 4.1. to help us to determine the Cl and Cd coefficients for a specific airfoil but the results were just auxiliary results and they are not shown in the tables.

CHAPTER 4. CFD ANALYSIS

4.1. Preliminary work

Before the calculation with the UAV models is run, it is compulsory to validate our computational results. The validation has to be done in order to make sure that all the data obtained from CFD looks similar to the real values obtained in the laboratory. As there are not real results of our models, the validation will be focused on different airfoils where empirical data is available. The values to compare with are extracted from the summary of airfoil data by Ira H. Abbott (see [18]) and they are going to be called as Theory results but they are empirical. In CFD is adequate to consider that the term similar means that the values only differ in a 20% of the reference value.

The airfoils NACA4412 and NACA0012 have been selected to run the previous simulations not only with Fluent but other programs like PABLO or XFOIL. The coordenate points of the NACA airfoils were obtained from [19].

As seen on sections 3.1. and 3.2. the grid is a very important factor in CFD because a small grid has more exactitude but makes the calculation slower and on the other hand, a grid where the points are separated a considerate distance makes the calculation faster but less exact. In Fig. 4.1 and Fig. 4.2 different quality grids are shown.

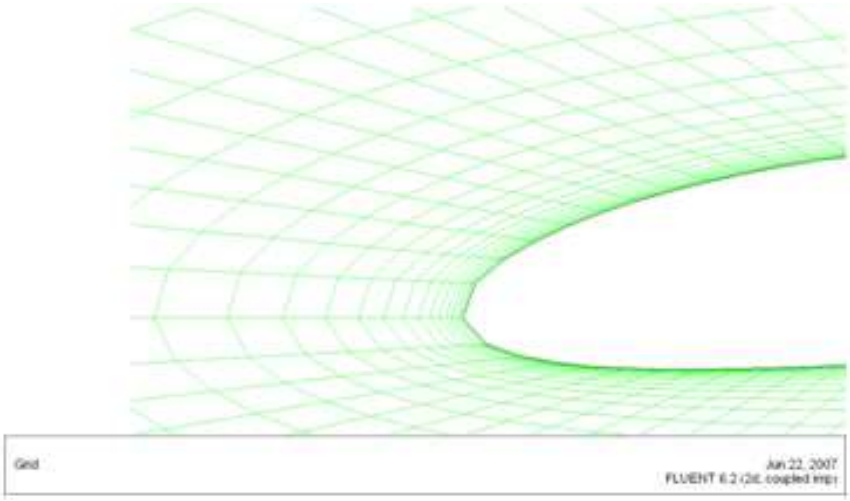

Figure 4.1: Coarse grid done with Gambit

Making a grid smaller will do our simulation better but there is a limit where making the grid smaller will not affect in the simulation except in the time cost to run it. In the Fig. 4.3 there are some results calculated with PABLO into a NACA4412 airfoil. The parameters of the graphics are different Reynolds, Cd and the quality of the mesh. The increment of points on the surface of the airfoil will do the simulation better but it only affects to the result in the first 50 points, after 50 points the result of the simulation is the same for more points. Then 50 points will be needed at least to make the simulations.

Fluent has a lot of variables to set up before running the simulation. Viscous model is

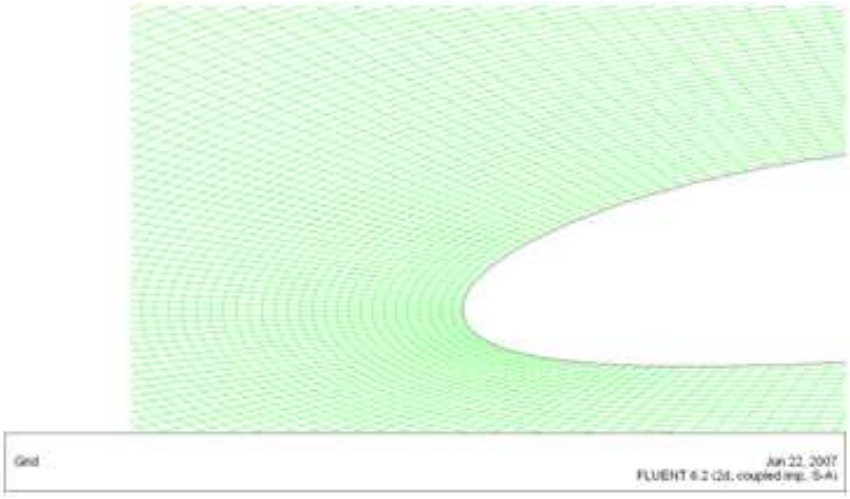

Figure 4.2: Fine grid done with Gambit

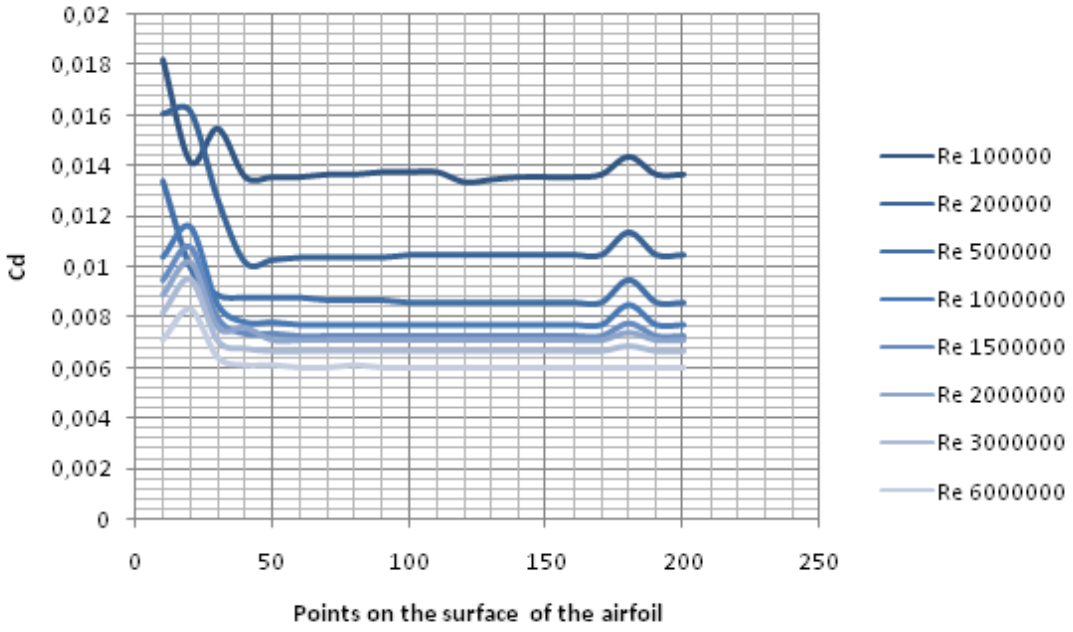

Figure 4.3: Graphic of Cd versus Quality of the mesh

a fundamental parameter in Fluent. First it is necessary to select the viscous model appropriate to our simulation. In order to validate the correctness of our choice, different simulations with different viscous models are shown in Table 4.1. These values represent the Cl and Cd coefficient for a NACA4412 airfoil at 0° angle of attack.

The values extracted from [18] are 0,4 and 0,006 for Cl and Cd respectively. The appropriate viscous model to choose is Spalart-Allmaras because the Cd values of the other simulations are far from the correct value although the inviscid result is the most approximate. This value is ruled out because the inviscid model does not take in account the drag caused by the friction of the wall of the airfoil and it is an unreal or utopian value. The Spalart-Allmaras [13] model was designed specifically for aerospace applications in-

Table 4.1: Results of Cl and Cd with different viscous models

Viscous model	Cl	Cd
Inviscid	0,5024	0,0089
Spalart-Allmaras	0,4306	0,0189
K - ε	0,3048	0,0892
K - ω	0,3956	0,0473

volving wall-bounded flows and has been shown to give good results for boundary layers subjected to adverse pressure gradients.

After determine the appropriate viscous model different simulations of a NACA0012 airfoil were done with different angles of attack. The results are compared with the Theory results and the results obtained with PABLO in Table 4.2. The Cl values look like the Theory values but the Cd does not.

Table 4.2: Cl and Cd values of a NACA0012 for different angles

Angles	Fluent Cl	Theory Cl	PABLO Cl	Fluent Cd	Theory Cd	PABLO Cd
-12°	-1,1411	-1,2750	-1,4217	0,0315	0,0160	0,016
-8°	-0,8016	-0,9000	-0,9527	0,0183	0,0100	0,0105
-4°	-0,4081	-0,4250	-0,4778	0,0141	0,0071	0,0074
0°	0,0011	0,0000	0,000	0,0133	0,0060	0,0066
4°	0,4081	0,4250	0,4778	0,0141	0,0071	0,0074
8°	0,8016	0,9000	0,9527	0,0183	0,0100	0,0105
12°	1,1411	1,2750	1,4217	0,0315	0,0160	0,016

If the Fluent Cd values are divided by the Theory values the number obtained is approximately equal to 2 ($\approx$ 1,97) for every number. Then, our Fluent result for Cd is always the double of the real value. The new values of Cd are shown in Table 4.3.

Table 4.3: Cd corrected values

Angles	Fluent Cd/2	Theory Cd	PABLO Cd
0°	0,0066	0,0060	0,0066
4°	0,0071	0,0071	0,0074
8°	0,0092	0,0100	0,0105
12°	0,0158	0,0160	0,016

In the Fig. 4.4a and Fig. 4.4b are shown the values from Table 4.2 and Table 4.3.

The error committed by our simulation referred to the Theory results is shown in Table 4.4. The absolute and the relative error have been calculated to estimate if our simulation with Fluent is enough accurate. The error committed is approximately of 10%. In conclusion, the simulation done with Fluent with the viscous model of Spallart-Allmarass can be considered as a good simulation.

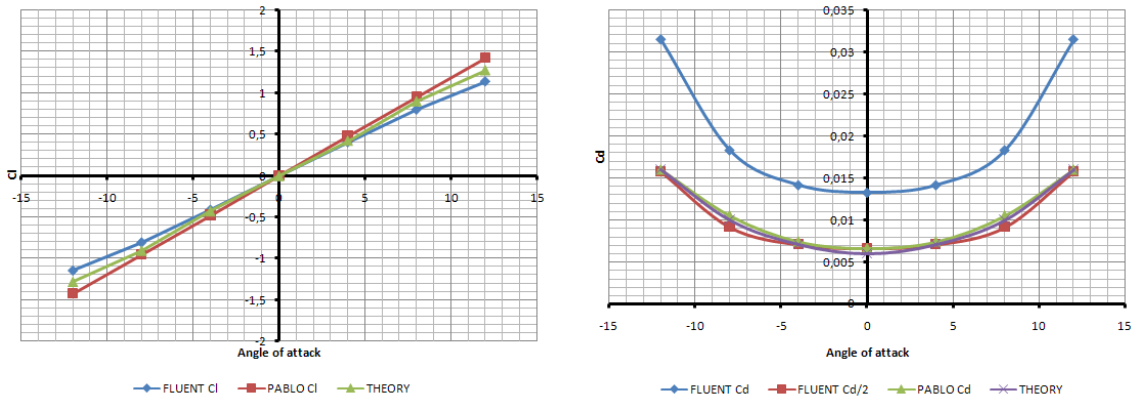

a) b)

Figure 4.4: a) Cl values versus angles of attack of a NACA0012. b) Cd versus angles of attack of a NACA0012

Table 4.4: Absolute and relative error of the coefficients calculated

Angles (°)	Cl Absolute error	Cd Absolute error	Cl Relative error (%)	Cd Relative error (%)
-12	0,1339	0,000249	10,50	1,56
-8	0,0984	0,000847	10,93	8,47
-4	0,0169	0,000025	3,97	0,36
0	0,0011	0,000631	0,11	10,52
4	0,0169	0,000025	3,97	0,36
8	0,0984	0,000847	10,93	8,47
12	0,1339	0,000249	10,50	1,56

As the validation has been completed in a suitable way, the simulations of the models shown in section 4.3. can be runned. The results obtained will be considered as correct results. The next results of Cd will be divided by 2 automatically.

4.2. UAV geometries

As seen on section 3.1. the first step in CFD is the generation of the mesh, but in order to generate the mesh, a model is needed. Then first of all, the geometries of the models have to be done.

As seen on section 1.2. there are two models to construct (Megastar and Shadow UAVs). This geometry of the Megastar is obtained directly from a previous TFC [20]. The geometry had to be updated because the motor was not implemented (see Fig.4.5).

The Shadow geometry had to be done completely. The drafts of Shadow were obtained directly from the constructor. Unfortunately the draft obtained had different measures from the real ones. Then, new measures had to be done at place. The finally geometry obtained can be viewed in Fig. 4.6.

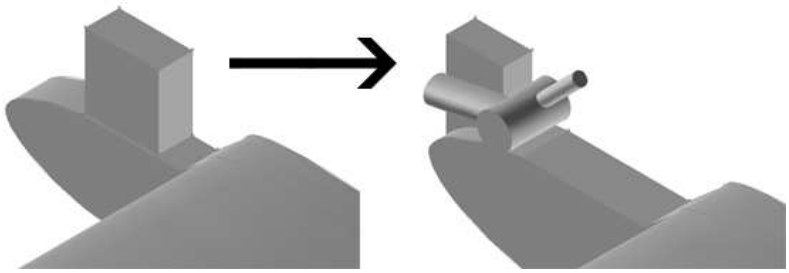

Figure 4.5: Engine implementation of Megastar

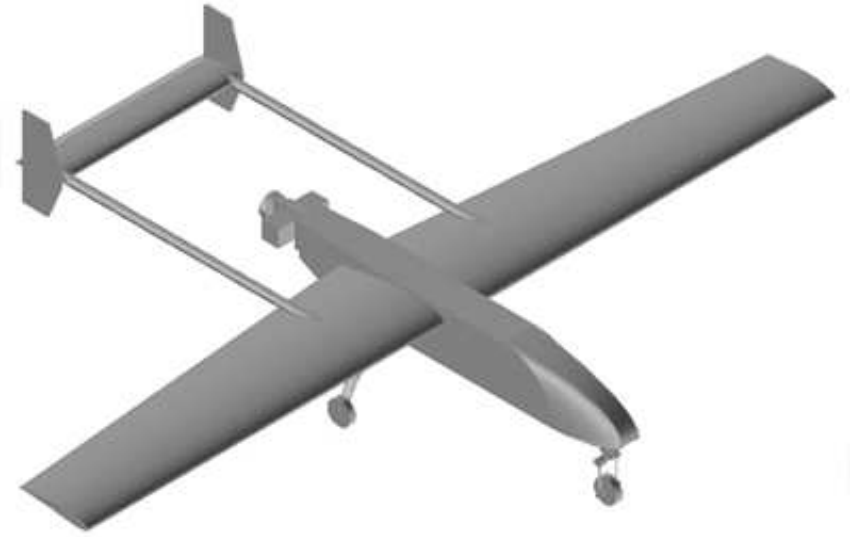

Figure 4.6: Geometry implementation of Shadow

4.3. Mesh modeling

As seen on section 3.1. a size function has to be implemented when the mesh is created. The parameters used for the size function are:

- Start size: 0.5
- Growth rate: 1.25
- Size limit: 25

The mesh obtained for Megastar and shadow are shown in Fig. 4.7 and Fig. 4.8. The total number of volumes created with this mesh are aproximately of 2.000.000. The boundary conditions applied to the model are the same as the explained in section 3.1..

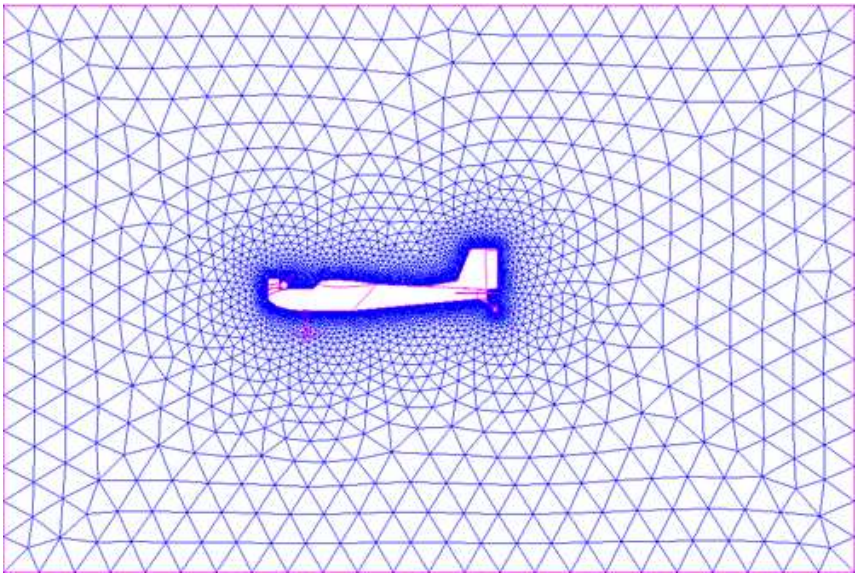

Figure 4.7: Mesh of the SYMMETRY section of the Megastar model

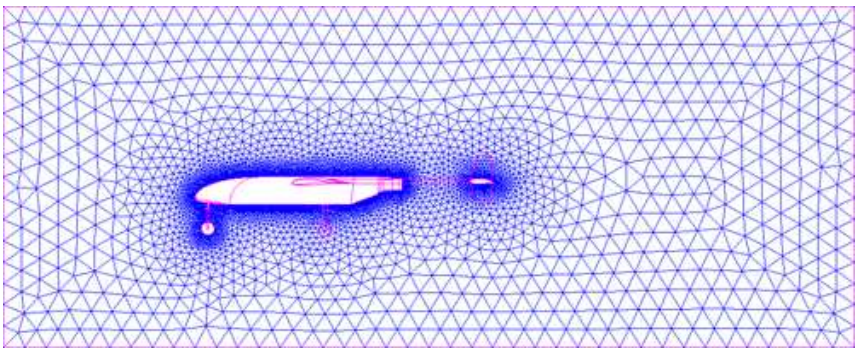

Figure 4.8: Mesh of the SYMMETRY section of the Shadow model

4.4. Results

This section will show the lift and drag coefficients extracted from Fluent as other CFD visual results. The models will be simulated in different angles of attack. The mesh shown in section 4.3. was implemented for a 0° angle of attack. New meshes have to be done in order to simulate the different angles of attack. Every simulation had up to 150 iterations and then converged.

The results shown below are all referred to the same area. By definition, the area of reference is the total surface of the wing. The values are classified in three groups, the contribution to Cl and Cd of the airfoil, the body, and the sum. The final value obtained is the coefficient of all the entire model of the UAV.

4.4.1. Megastar coefficients

The Table 4.5 shows the different lift and drag results obtained from Fluent.

Table 4.5: Lift and drag coefficients for different angles of attack of the UAV Megastar

Angles	Airfoil Cl	Airfoil Cd	Body Cl	Body Cd	Megastar Cl	Megastar Cd
-12°	-0,7415	0,0438	-0,1565	0,0355	-0,8980	0,0793
-8°	-0,4823	0,0235	-0,1062	0,0264	-0,5885	0,0499
-4°	-0,2033	0,0139	-0,0576	0,0213	-0,2609	0,0352
0°	0,0747	0,0119	-0,0085	0,0198	0,0662	0,0317
4°	0,3537	0,0177	0,0439	0,0210	0,3976	0,0388
8°	0,6275	0,0329	0,0969	0,0259	0,7244	0,0588
12°	0,8701	0,0573	0,1484	0,0347	1,0185	0,0920
16°	1,0797	0,1038	0,2029	0,0475	1,2826	0,1513
20°	1,3089	0,2003	0,2571	0,0652	1,5660	0,2655
21°	1,3625	0,2347	0,2679	0,0696	1,6304	0,3043
22°	1,4070	0,2688	0,2777	0,0771	1,6847	0,3432
23°	1,3959	0,2898	0,2850	0,0790	1,6809	0,3688
24°	1,4177	0,3161	0,2959	0,0842	1,7136	0,4003
25°	1,3834	0,3309	0,3016	0,0890	1,6850	0,4199
26°	1,2936	0,3314	0,3095	0,0949	1,6032	0,4263

The Fig. 4.9a shows the Cl values from the Table 4.5 versus the angle of attack. Between -12° and 20° Cl is linear and next Cl starts to decrease, the model is in the stall condition. The Fig. 4.9b shows the Cd values from the Table 4.5 versus the angle of attack. Cd graphics have a parabolic profile.

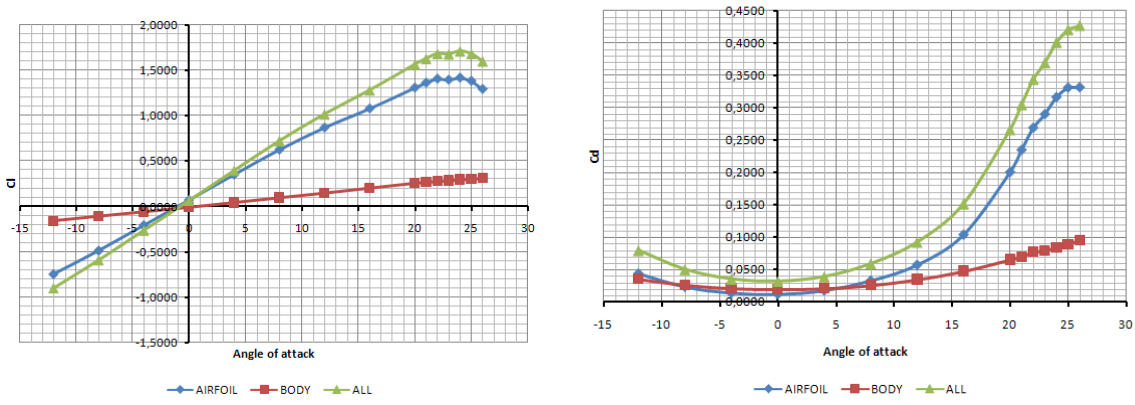

a) b)

Figure 4.9: a) Cl versus angle of attack. b) Cd versus angle of attack

The Fig. 4.10 shows the Cd values from the Table 4.5 versus the Cl coefficient. As Cl decreases in the final angles of attack, Cd has a backward movement with high values of Cl.

As previous commented in 2.1.3. the aerodynamic efficiency is calculated by dividing Cl/Cd. Fig. 4.11 shows this ratio for every calculated angle of attack. The maximum aerodynamic efficiency and consequently the maximum gliding range is obtained with the angle of attack of 8°.

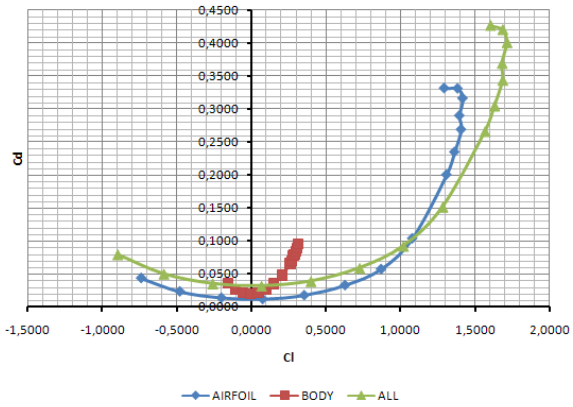

Figure 4.10: Graphic of Cd versus Cl

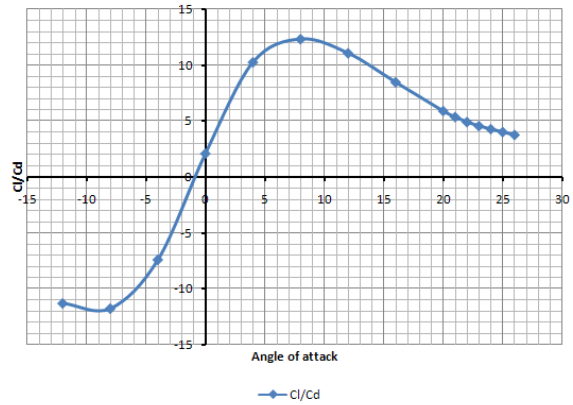

Figure 4.11: Graphic of Cl/Cd ratio versus angle of attack

The optimum parameters of Megastar are shown in table 4.6. The optimum value for the velocity of the UAV is calculated for two different values of the vehicle weight. As the final weight of the UAV is unknown, the value used for the weight are the zero fuel weight (ZFW) and the maximum take off weight (MTOW). These values are the minimum and maximun weights respectively that an aircraft can weigh. As seems logical, more weight involves more velocity.

Table 4.6: Optimum parameters for maximum (L/D) ratio for the UAV Megastar

Angle of attack	8°	
Cl	0,7244	
Cd	0,0588	
Maximum (L/D) ratio	12,32	
	Vehicle weight	**Velocity**
ZFW	7 Kg	12,83 m/s
MTOW	14 Kg	18,15 m/s

4.4.1.1. Equations of the coefficients

The Eqs 4.2 to 4.3 are the approximate trend line of the Cl versus angle of attack shown in Fig. 4.9a.

$$Cl_{Airfoil} = 0,06796\alpha + 0,07128 \tag{4.1}$$
$$Cl_{Body} = 0,01270\alpha - 0,00567 \tag{4.2}$$
$$Cl_{Megastar} = 0,08066\alpha + 0,06561 \tag{4.3}$$

The Eqs 4.5 to 4.6 are the approximate trend line of the Cd versus angle of attack shown in Fig. 4.9b.

$$Cd_{Airfoil} = 0,00027\alpha^2 + 0,00056\alpha + 0,01142 \tag{4.4}$$
$$Cd_{Body} = 0,00011\alpha^2 - 0,00003\alpha + 0,01950 \tag{4.5}$$
$$Cd_{Megastar} = 0,00038\alpha^2 + 0,00053\alpha + 0,03092 \tag{4.6}$$

All these equations can be used by the autopilot. The equations permits to obtain an approximate result of the coefficient for almost every angle of attack.

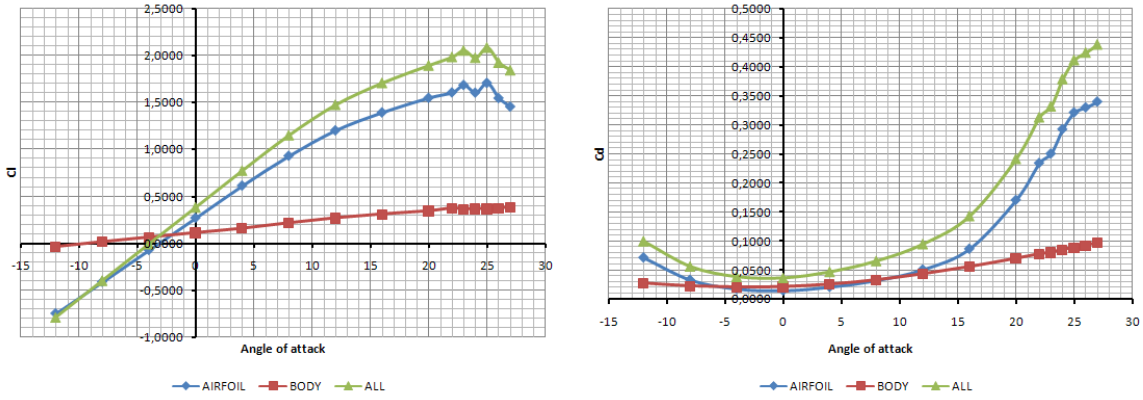

a) b)

Figure 4.12: a) Cl versus angle of attack. b) Cd versus angle of attack

4.4.2. Shadow coefficients

The Table 4.7 shows the different lift and drag results obtained from Fluent for the different reference values.

The Fig. 4.12a shows the Cl values from the Table 4.7 versus the angle of attack. The Fig. 4.12b shows the Cd values from the Table 4.7 versus the Cl coefficient. The Fig. 4.13 shows the Cd values from the Table 4.7 versus the angle of attack.

Table 4.7: Lift and drag coefficients for different angles of attack of the UAV Shadow

Angles	Airfoil Cl	Airfoil Cd	Body Cl	Body Cd	Shadow Cl	Shadow Cd
-12°	-0,7495	0,0714	-0,0307	0,0282	-0,7834	0,0996
-8°	-0,4124	0,0329	0,0208	0,0232	-0,3916	0,0561
-4°	-0,0722	0,0173	0,0698	0,0213	-0,0024	0,0386
0°	0,2691	0,0144	0,1168	0,0221	0,3859	0,0364
4°	0,6132	0,0206	0,1631	0,0263	0,7763	0,0469
8°	0,9308	0,0319	0,2206	0,0337	1,1515	0,0656
12°	1,2022	0,0507	0,2729	0,0440	1,4751	0,0947
16°	1,3936	0,0864	0,3137	0,0564	1,7073	0,1428
20°	1,5488	0,1706	0,3479	0,0706	1,8935	0,2411
22°	1,6068	0,2342	0,3767	0,0783	1,9835	0,3125
24°	1,6045	0,2925	0,3708	0,0859	1,9753	0,3784
25°	1,7081	0,3214	0,3715	0,0895	2,0830	0,4109
26°	1,5461	0,3300	0,3773	0,0930	1,9234	0,4238
27°	1,4555	0,3400	0,3860	0,0977	1,8415	0,4377

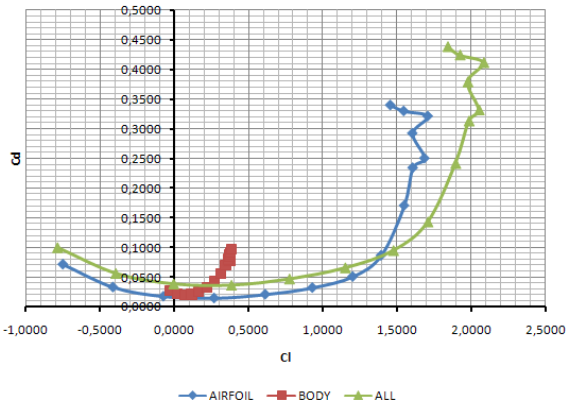

Figure 4.13: Graphic of Cd versus Cl

As previous commented with Megastar in 4.4.1., Fig. 4.11 shows the Cl/Cd ratio for every calculated angle of attack. The maximum aerodynamic efficiency and consequently the maximum gliding range is obtained with the angle of attack of 7°.

The optimum parameters of Shadow are shown in table 4.8.

4.4.2.1. Equations of the coefficients

The Eqs 4.8 to 4.9 are the approximate trend line of the Cl versus angle of attack shown in Fig. 4.12a.

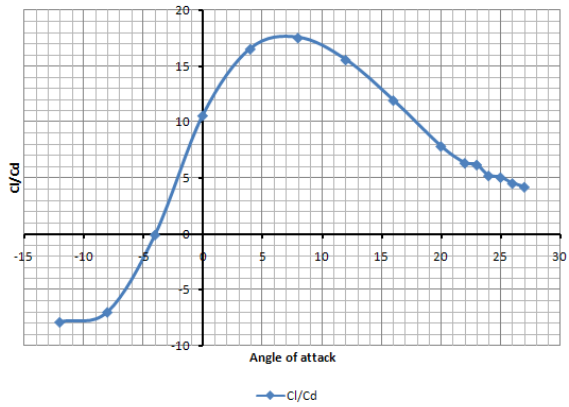

Figure 4.14: Graphic of Cl/Cd ratio versus angle of attack

Table 4.8: Optimum parameters corresponding to the maximum (L/D) ratio for the UAV Shadow

Angle of attack	7°	
Cl	1,3133	
Cd	0,0662	
Maximum (L/D) ratio	19,84	
	Vehicle weight	**Velocity**
ZFW	55 Kg	15,48 m/s
MTOW	90 Kg	19,80 m/s

$$Cl_{Airfoil} = 0,08238\alpha + 0,25447 \tag{4.7}$$

$$Cl_{Body} = 0,01253\alpha + 0,11904 \tag{4.8}$$

$$Cl_{Shadow} = 0,09500\alpha + 0,37305 \tag{4.9}$$

The Eqs 4.8 to 4.9 are the approximate trend line of the Cl versus angle of attack shown in Fig. 4.12b.

$$Cl_{Airfoil} = 0,0000005482\alpha^4 - 0,0000099995\alpha^3 \tag{4.10}$$
$$+0,0002426004\alpha^2 + 0,0005768566\alpha + 0,0147087122$$

$$Cl_{Body} = 0,0000966929\alpha^2 + 0,0006570834\alpha + 0,0222144926 \tag{4.11}$$

$$Cl_{Shadow} = 0,0000005148\alpha^4 - 0,0000098366\alpha^3 \tag{4.12}$$
$$+0,0003444093\alpha^2 + 0,0012156998\alpha + 0,0368352438$$

4.5. Graphics and visualization

As a CFD simulation calculates every physical parameter in every point of the grid, CFD permits to show different visual results in function of the physical variable selected. Fluent is a powerful utility to present aerodynamics and heat transfer works in a visual way. The next sections shows differents visual results obtained with Fluent.

4.5.1. Contours

The contours results allows to plot contour lines or profiles superimposed on the physical domain. Contour lines are lines of constant magnitude for a selected variable (isotherms, isobars, etc.). A profile plot draws these contours projected off the surface along a reference vector by an amount proportional to the value of the plotted variable at each point on the surface.

The contours of dynamic pressure of the model Shadow is shown in Fig. 4.15 and 4.16. As seen on the scale, the values are higher on the upper faces than the lower faces. As seen on section 2.1.1. this difference of pressures will generate the lift force.

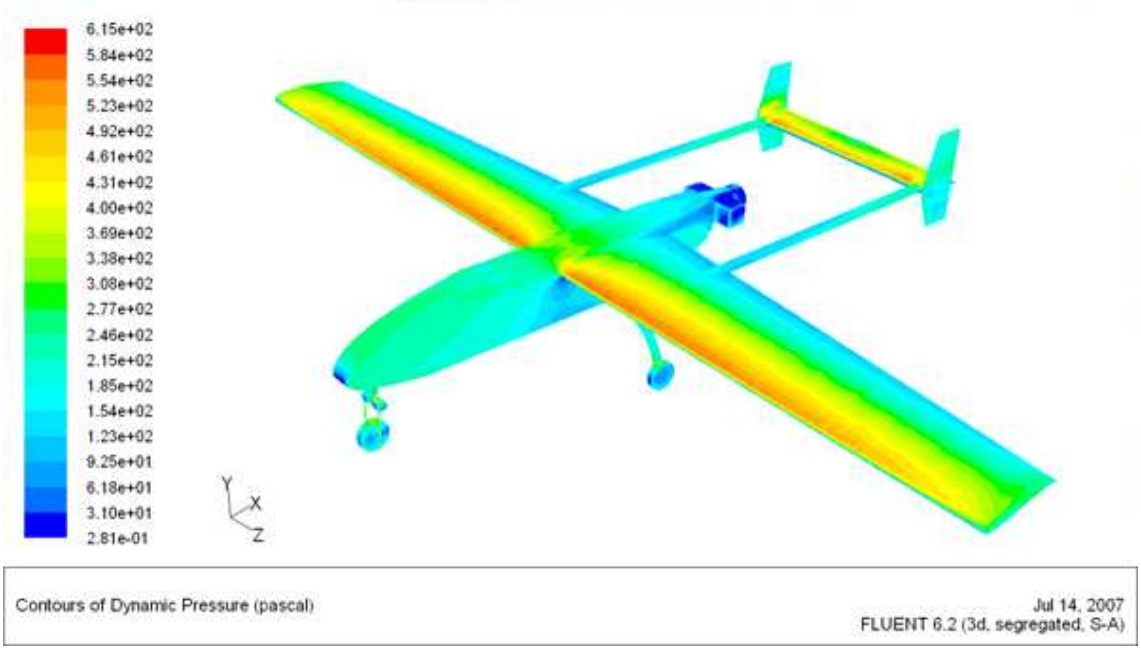

Figure 4.15: Contours of dynamic pressure of the model Shadow

4.5.2. Vectors

By default, one vector is drawn at the center of each cell, with the length and color of the arrows representing the velocity magnitude. The spacing, size, and coloring of the arrows can be modified, along with several other vector plot settings. Velocity vectors are the default, but it is also possible to plot vector quantities other than velocity.

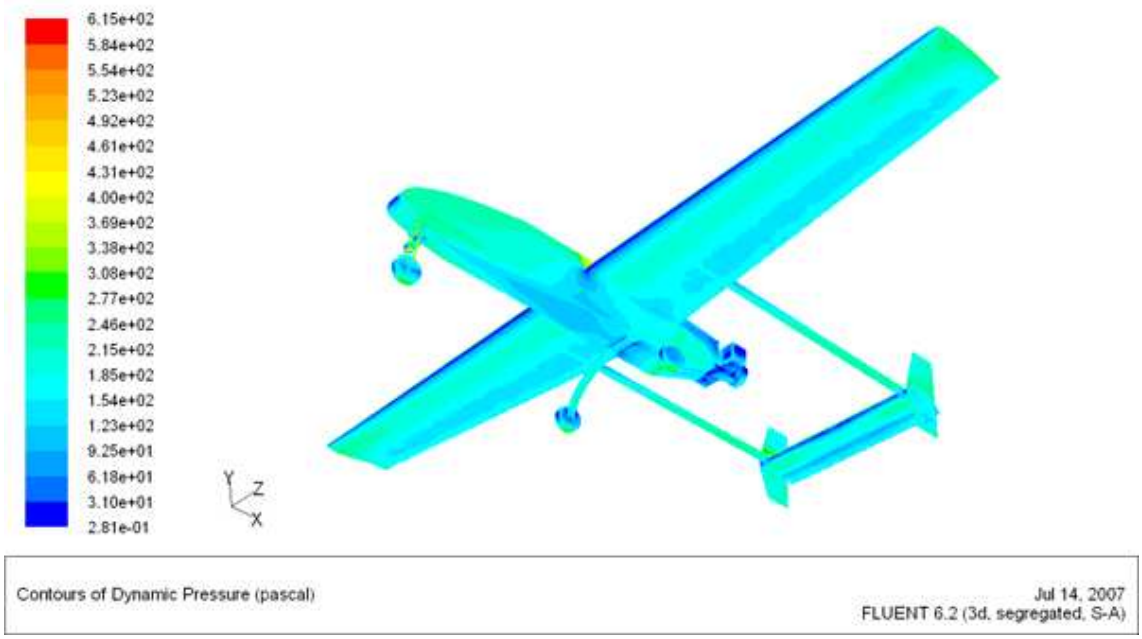

Figure 4.16: Contours of dynamic pressure of the model Shadow

The velocity vectors on the symmetry plane are shown in Fig. 4.17. The visualization is focused on the rear of the motor. Here, a vortex is created. The vortex will affect negatively to the lift force. This kind of visualization helps engineers to implement new geometries to improve aerodynamic forces.

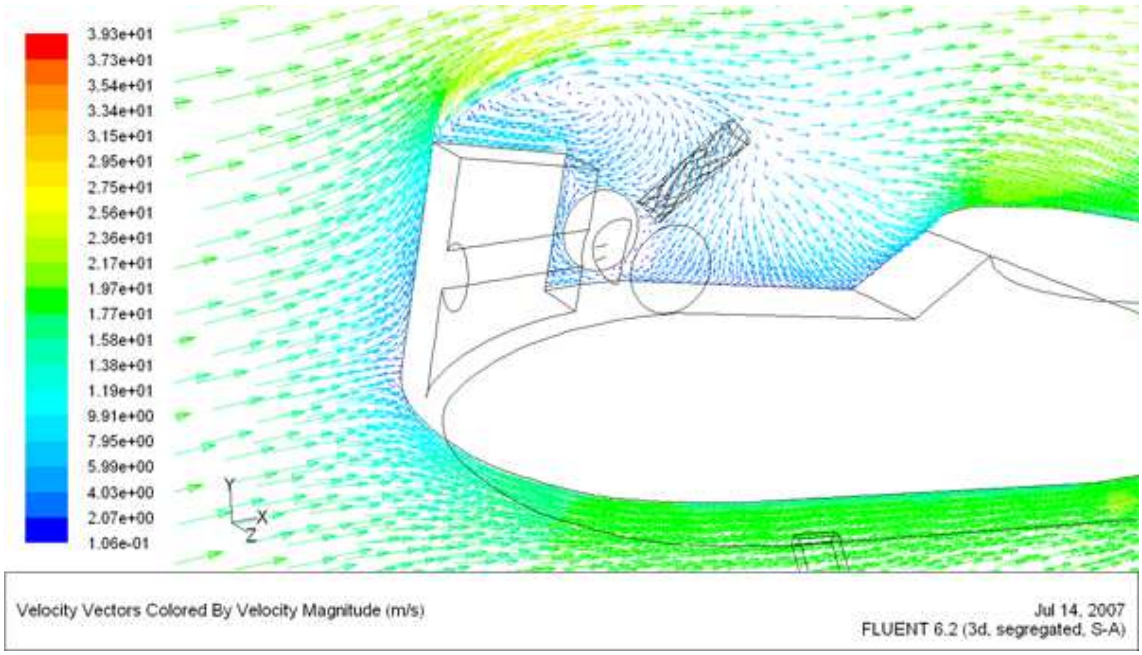

Figure 4.17: Velocity vectors on the symmetry plane of the model Megastar

4.5.3. Pathlines

Pathlines are used to visualize the flow of massless particles in the problem domain. The particles are released from one or more surfaces created with Fluent.

Diverses path lines crossing the airfoil are shown on Fig. 4.18. Path lines may show a vortex generated on the edge of the airfoil.

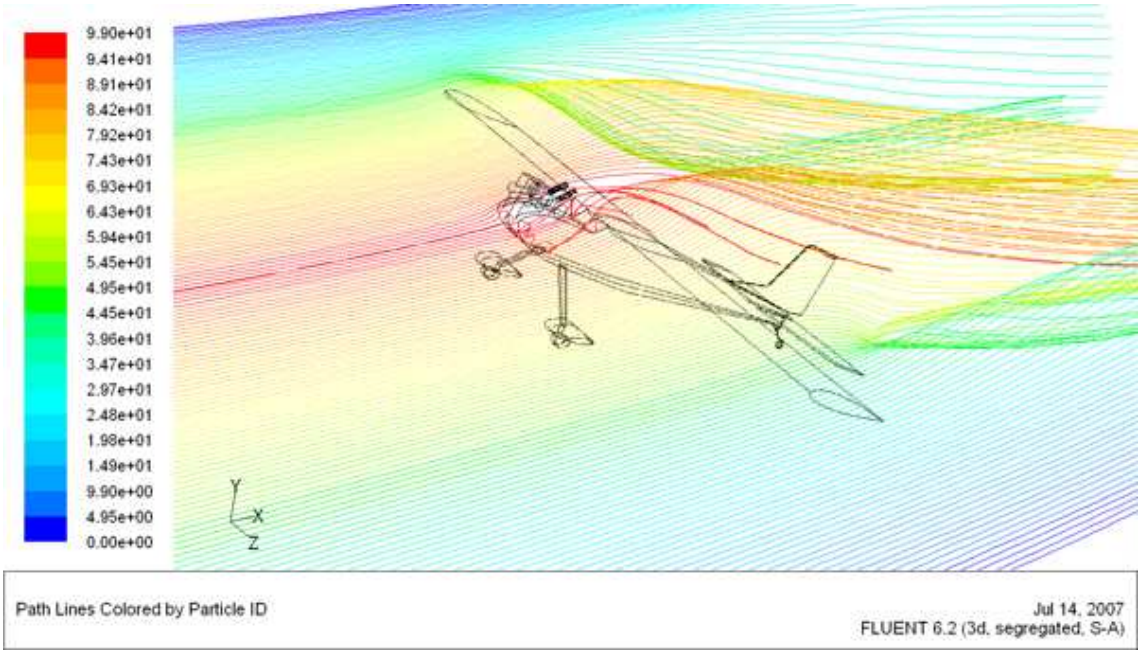

Figure 4.18: Path lines on the plane crossing the airfoil of the model Megastar

4.5.4. XY Plots

In addition to the many graphics tools already discussed, Fluent also provides tools to generate XY plots and histograms of solution, file, and residual data.

An example of a XY plot is shown in Fig. 4.19 and Fig. 4.20. These plots have been done on a line created over and under the airfoil. Dynamic and static pressure are shown. As seen in section 2.1.1., when the static pressure increases, the dynamic pressure decreases and viceversa in order to mantain the total pressure constant.

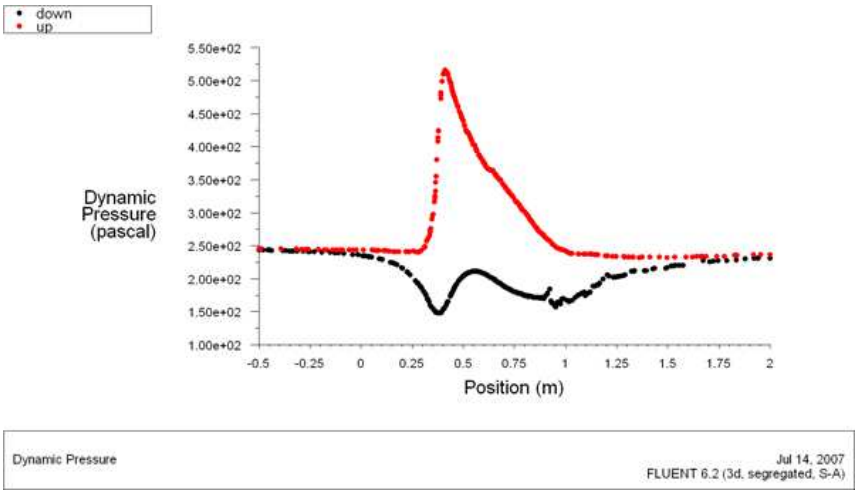

Figure 4.19: XY plot of the dynamic pressure of a section of the airfoil of the model Shadow

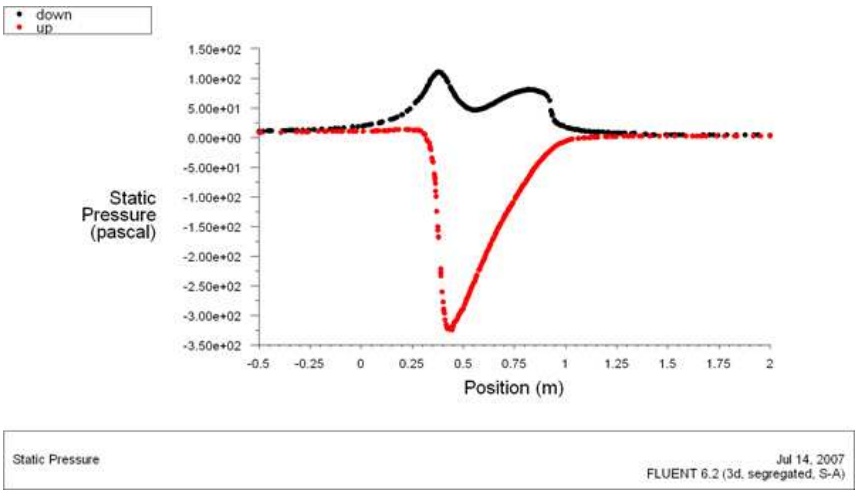

Figure 4.20: XY plot of the static pressure of a section of the airfoil of the model Shadow

CHAPTER 5. DATCOM

5.1. Inputs

As it has been said in previous sections, the USAF Datcom needs an input file in order to calculate all aircraft performance characteristics. In this input file, which is not very user friendly, it should be specified all the geometric characteristics of the aircraft and other variables needed to simulate it. All the parameters have been obtained from real measurements done in the laboratory except the vehicle weight that has been obtained from the datasheet. There are four big data groups in the input file:

- Flight conditions and reference dimensions
- Basic geometry configuration
- Additional configuration definition
- Execution control and special options

Although in each group there is an extensive data list, it is not necessary to specify all of them. Much of the data that is required for subsonic simulations for example, it is not required for hypersonic or transonic ones. As this example, there are a lot more that considerably reduce the data inputs. The simulations of this project refer to a subsonic body-wing-horizontal-vertical geometry simulation.

The first group is divided into two: flight conditions and reference dimensions. In both simulations (Megastar and Shadow), are specified the same type of data. For the flight conditions we have to indicate the information below:

- Number and value of the Mach numbers to be run
- Number and value of the altitudes to be run
- Number and value of the angles of attack to be run
- Upper and lower limit of mach numbers of subsonic and hypersonic simulations respectively
- Vehicle weight (in Newtons)

The reference dimensions need less data than the upper one, but there are not less important. The following variables are the ones required for the simulation:

- Surface roughness factor
- Reference area (wing area)

- Reference chord
- Reference wing span

The second big group is probably the larger one. In it, there are the basic geometry properties of the aircraft. It is structured in different kinds of parameters: the synthesis parameters, the body configuration and the planform geometry for each of the aerodynamic surfaces (wing, horizontal tail, vertical tail and ventral fin). In the Megastar and the shadow simulation, the data required is the following one:

- Longitudinal and vertical location of the centre of gravity
- Longitudinal and vertical location of the wing apex)
- Wing root chord incidence angle
- Longitudinal and vertical location of the horizontal tail apex
- Horizontal tail root chord incidence angle
- Longitudinal and vertical location of the vertical tail apex
- Vehicle scale factor

Most of the data inputs for the body geometry are extracted from transversal cuts of the fuselage in the longitudinal axis. The other variables are the type and the method of the simulation, which refers to the shape of the body (circular, elliptic or others). In resume, these are the data inputs:

- Number of longitudinal body station at which data is specified
- Longitudinal distance
- Cross sectional area
- Periphery at station
- Half width at station
- Upper and lower limits of the station
- Type and method of the simulation

The last data of this group is the one referred to the planform geometry of each of the aerodynamic surfaces. Nearly all the data is the same for all the surfaces, although it is probably that some of it will not be needed. Both the Megastar and the Shadow have a wing, a horizontal tail and a vertical tail and neither of them have a ventral fin. The data required for this sub-group is the following one:

- Tip chord
- Root chord
- Chord at breakpoint (if there is a breakpoint)
- Semi-span outboard, exposed and theoretical panel
- Inboard and outboard panel sweep angle
- Dihedral angle of inboard and outboard panel

It is necessary to specify all the characteristics of the airfoil of each surface. There is a lot of data needed for this reason but it is an excellent recommendation to specify what NACA airfoil is.

The next big group defines the additional configuration geometry. In this group there are a lot of possible combinations to simulate but in the simulation of this project are needed a fewer of them Both the Megastar and the Shadow have symmetrical hyper sustentation devices: the elevators, but only the Shadow has ailerons (asymmetrical). In addition, it should be indicated that the Shadow has twin vertical panels which should be specified. The data required for the twin vertical panels is:

- Vertical panel span above lifting surface
- Vertical panel span
- Fuselage depth
- Distance between panels
- Planform area of one panel
- Total trailing edge angle
- Longitudinal and vertical distance to the centre of gravity

For the aileron, this is the data that should be specified:

- Type of aileron
- Number and values of the control deflection angles
- Span location of inboard end of the aileron
- Span location of outboard end of the aileron
- Tangent of airfoil trailing edge
- Aileron chord at inboard end of plain flap aileron
- Aileron chord at outboard end of plain flap aileron

Finally, the data required for the elevators is:

- Type of elevator
- Number and values of the control deflection angles
- Span location of inboard end of elevator
- Span location of outboard end of elevator
- Tangent of airfoil trailing edge at 90 and 99 per cent chord
- Tangent of airfoil trailing edge at 95 and 99 per cent chord
- Elevator chord at inboard end of plain flap elevator
- Elevator chord at outboard end of plain flap elevator
- Average chord
- Average thickness

The last group is the execution control. The user can specify what type of simulation wants, the system units or the control execution parameters. In the simulations of this project, the system units are defined to centimetres and degrees. In addition, the program, allows the user to specify the name of the aircraft and of the different lifting surfaces. At last, it should be remarked that is in this section where the NACA airfoils are defined and not in the second group.

5.2. Outputs

The first software of the USAF Datcom only provided a fewer outputs files which were not very user friendly. Nowadays, new tools have been added to the software in order to make it more friendly and useful.

Basically, there were only two outputs files in the USAF Datcom: a plot one and another one that could be opened with spreadsheet applications. The plot one (lfiplot), print the graphics in the screen but it not allows the user to manage it much. In the excel file, there is an error inform that can point out what type of error is and where it has occurred. It also contains tables for all the coefficients.

The newer version also contains these two useful files but it also has two more that provide efficient simulations and results. There is a file for the three dimensional visualization of the aircraft model and a plot file much more friendly and manageable than the first one.

In this section, there is an extensive and efficient report of the results obtained from the Datcom simulations.

In order to have good simulations, it is important to specify the limitations of this software. Firstly, the body configuration and parameters are an approximation of the real model due to it is very difficult to have values of the aircraft in each centimetre of the model; there is a maximum of 20 longitudinal sections to specify. Moreover, the addition of a landing gear is completely impossible since the software does not have this option. There are other errors that could be a fault of the software itself or of the visualization tools; some distances well defined in the input file, do not appear well in the visualization tool and the body geometry is always cylindrical although the program has the option to define a special geometry. For these reasons, the results of the simulations should be analyzed in an intelligent way because it could exist the possibility that the results could have errors although they would be very little.

All coefficient that are shown in the tables are refferred by an acronym and the complete meaning of the coefficients is explained in table 5.1.

Table 5.1: Acronyms of the aerodynamic coefficients

CL	Lift coefficient
CD	Drag coefficient
CM	Moment coefficient
CN	Normal Force coefficient
CA	Axial force coefficient
CYB	Yawing moment coefficient due to sideslip
CNB	Side force coefficient due to sideslip
CLB	Rolling moment coefficient due to sideslip
CLQ	Lift coefficient due to pitch rate derivative
CMQ	Pitching moment coefficient due to pitch rate derivative
CLAD	Lift coefficient due to angle of attack rate derivative
CMAD	Pitching moment coefficient due to angle of attack rate derivative
CLP	Rolling moment coefficient due roll rate derivative
CYP	Yawing moment coefficient due roll rate derivative
CNP	Side force coefficient due roll rate derivative
CNR	Side force coefficient due yaw rate derivative
CLR	Rolling moment coefficient due yaw rate derivative

5.2.1. Megastar results

Due to the difficult to know if an input file is correctly done, is needed a visualization of our file through the visualization tool. In Fig. 5.1, there is the aircraft visualization with the magnitudes given in the input file. There are some qualities of the aircraft that are not correctly drawn. For example, the tip chord of the horizontal tail has not the correct value because the program picks up the value of the tip chord of the wing. After lots of simulations the conclusion is that the visualization tool is the one that does not pick the correct value, but the results in the other output files are with the correct values so the problem is not so serious.

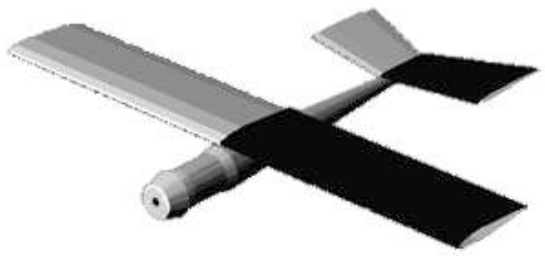

Figure 5.1: Megastar visualization through the Datcom tool

In order to visualize the results in a clear way, there are tables above were the different coefficients are shown in each angle of attack.

The table 5.2 shows the longitudinal coefficients obtained in the Datcom simulations for each angle of attack.

Table 5.2: Datcom longitudinal coefficients for the Megastar

Angles	**CL**	**CD**	**CM**	**CN**	**CN**
-12°	-1,003	0,081	-0,6568	0,998	-0,129
-8°	-0,618	0,043	-0,3843	0,618	-0,043
-4°	-0,264	0,025	-0,1363	0,265	0,007
0°	0,069	0,021	0,0867	0,069	0,021
4°	0,419	0,031	0,3405	0,42	0,001
8°	0,796	0,058	0,6107	0,796	-0,053
12°	1,191	0,105	0,93	1,187	-0,145
16°	1,5	0,158	1,0302	1,485	-0,262
20°	1,69	0,203	1,0059	1,657	-0,387
21°	1,707	0,21	0,9718	1,669	-0,415
22°	1,667	0,207	0,9097	1,623	-0,432
23°	1,612	0,203	0,8328	1,563	-0,443
24°	1,276	0,16	0,5176	1,231	-0,373
25°	0,88	0,123	0,2097	0,85	-0,261
26°	0,507	0,099	-0,015	0,499	-0,134

One of the advantages of the software is that many coefficients are obtained from an approximate geometry. In this way, tables 5.3 and 5.4 show the derivatives obtained from the Datcom simulations for each angle of attack.

The Datcom also simulate the aircraft in other more situations like the deflection of its lift devices. In this way, in the table 5.5, there are the increments due to the deflection of the elevator, the only lift device of the Megastar because the rudder cannot be simulated through this software.

At last, Fig. 5.2a, Fig. 5.2b and Fig. 5.3, illustrate in a clearly way the results obtained for the Cl and the Cd, the most common aerodynamic coefficients.

Table 5.3: Datcom derivatives coefficients for the Megastar (part 1)

Angles	CYB	CNB	CLB	CLQ	CMQ	CLR
-12°	-5,16E-03	-5,93E-04	1,08E-03	-4,88E-02	-1,18E-01	-3,57E-03
-8°	-5,16E-03	-5,93E-04	5,07E-04	-4,88E-02	-1,18E-01	-2,14E-03
-4°	-5,16E-03	-5,93E-04	-3,33E-05	-4,88E-02	-1,18E-01	-7,93E-04
0°	-5,16E-03	-5,93E-04	-5,21E-04	-4,88E-02	-1,18E-01	4,27E-04
4°	-5,16E-03	-5,93E-04	-1,03E-03	-4,88E-02	-1,18E-01	1,71E-03
8°	-5,16E-03	-5,93E-04	-1,59E-03	-4,88E-02	-1,18E-01	3,11E-03
12°	-5,16E-03	-5,93E-04	-2,17E-03	-4,88E-02	-1,18E-01	4,56E-03
16°	-5,16E-03	-5,93E-04	-2,58E-03	-4,88E-02	-1,18E-01	5,59E-03
20°	-5,16E-03	-5,93E-04	-2,76E-03	-4,88E-02	-1,18E-01	6,08E-03
21°	-5,16E-03	-5,93E-04	-2,73E-03	-4,88E-02	-1,18E-01	6,05E-03
22°	-5,16E-03	-5,93E-04	-2,62E-03	-4,88E-02	-1,18E-01	5,80E-03
23°	-5,16E-03	-5,93E-04	-2,48E-03	-4,88E-02	-1,18E-01	5,48E-03
24°	-5,16E-03	-5,93E-04	-1,89E-03	-4,88E-02	-1,18E-01	3,92E-03
25°	-5,16E-03	-5,93E-04	-1,23E-03	-4,88E-02	-1,18E-01	2,25E-03
26°	-5,16E-03	-5,93E-04	-6,51E-04	-4,88E-02	-1,18E-01	7,98E-04

Table 5.4: Datcom derivatives coefficients for the Megastar (part 2)

Angles	CLAD	CMAD	CLP	CYP	CNP	CNR
-12°	2,14E-02	-3,20E-02	-8,73E-03	-1,50E-03	1,23E-03	-8,72E-04
-8°	2,02E-02	-3,03E-02	-8,17E-03	-9,40E-04	7,65E-04	-6,91E-04
-4°	2,28E-02	-3,41E-02	-7,54E-03	-4,02E-04	3,16E-04	-6,08E-04
0°	-2,26E-02	-3,38E-02	-7,37E-03	1,04E-04	-1,06E-04	-6,06E-04
4°	2,22E-02	-3,32E-02	-7,89E-03	6,31E-04	-5,46E-04	-6,76E-04
8°	2,15E-02	-3,22E-02	-8,39E-03	1,19E-03	-1,01E-03	-8,37E-04
12°	1,81E-02	-2,72E-02	-7,42E-03	1,78E-03	-1,55E-03	-1,10E-03
16°	1,16E-02	-1,73E-02	-4,76E-03	2,28E-03	-2,06E-03	-1,34E-03
20°	1,92E-03	-2,88E-03	-5,72E-04	2,66E-03	-2,44E-03	-1,48E-03
21°	9,53E-04	1,43E-03	2,73E-03	2,80E-03	-2,52E-03	-1,47E-03
22°	1,56E-02	2,34E-02	6,04E-03	3,10E-03	-2,28E-03	-1,39E-03
23°	2,81E-02	4,21E-02	2,08E-02	2,30E-03	-3,33E-03	-1,31E-03
24°	5,14E-02	7,70E-02	3,61E-02	1,99E-03	-2,92E-03	-9,56E-04
25°	6,56E-02	9,83E-02	3,49E-02	1,55E-03	-1,75E-03	-7,03E-04
26°	5,58E-02	8,35E-02	2,99E-02	1,13E-03	-9,48E-04	-5,87E-04

Table 5.5: Increments due to the deflection of the elevator in the Megastar

Delta	D(CL)	D(CM)	D(CL MAX)	D(CD MIN)
-31°	-0,13	0,2048	0,135	0,01175
0°	0	-0,0001	0	0
25°	0,118	-0,1842	0,117	0,0079

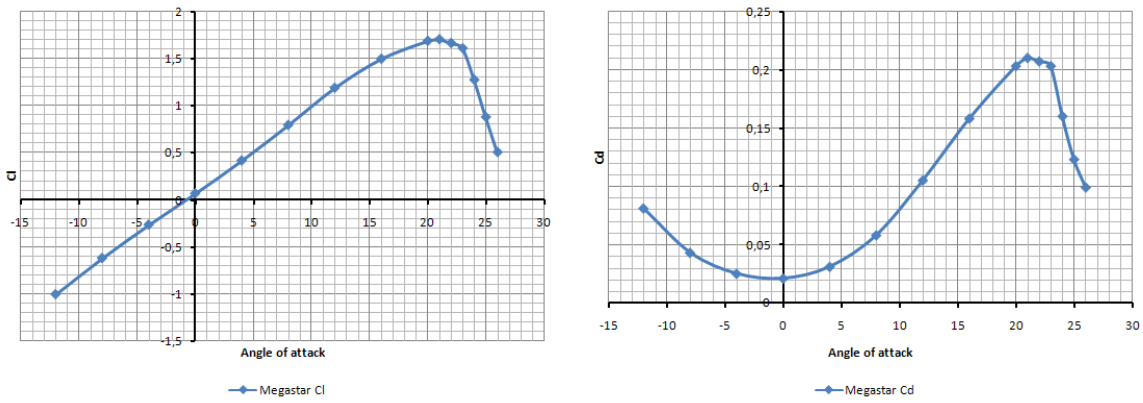

a) b)

Figure 5.2: a) Cl values from table 5.2 versus angle of attack. b) Cd values from table 5.2 versus angle of attack.

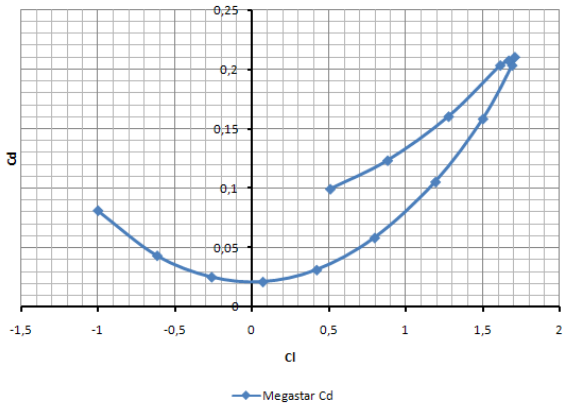

Figure 5.3: Cd values from table 5.2 versus Cl values of the same table

The Datcom simulations show that the aircraft critical angle of attack is 21^{o}. In this angle, the aircraft is in stall and because of this, after this angle, the graphics of all the coefficients begin to do strange things. It is good to say that it is not a problem the values obtained in that zone, so the study, compares and analyzes the values up to 21^{o}.

5.2.2. Shadow results

The same problems of the Megastar simulations occur in the Shadow ones, and for this reason, there are done the same steps in order to show the results obtained. The figure 5.4 shows the visualization of the Shadow with the geometry inputs given. No vertical fins are drawn although they are specified in the input file. There is only one longitudinal pipe uniting the body-wing and the horizontal tail and is due to the problems to specify two pipes in the same section.

The table 5.6 shows the longitudinal coefficients obtained in the Datcom simulations for each angle of attack.

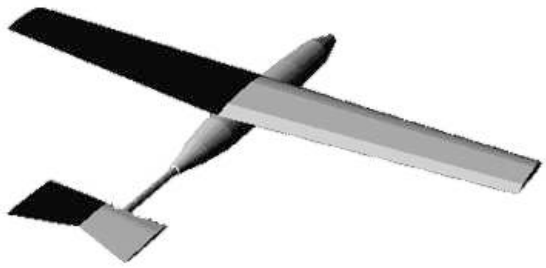

Figure 5.4: Shadow visualization through the Datcom tool

Table 5.6: Datcom longitudinal coefficients for the Shadow

Angles	CL	CD	CM	CN	CN
-12°	-0,709	0,039	-0,6673	-0,701	-0,109
-8°	-0,334	0,023	-0,3868	-0,334	-0,023
-4°	0,019	0,019	-0,1367	0,018	0,02
0°	0,376	0,025	0,1171	0,376	0,025
4°	0,759	0,042	0,4012	0,76	-0,011
8°	1,163	0,074	0,6982	1,162	-0,088
12°	1,497	0,112	0,9718	1,488	-0,202
16°	1,694	0,142	1,1504	1,668	-0,331
18°	1,69	0,146	NA	1,653	-0,383
20°	1,438	0,123	NA	1,393	-0,376

There are values that are not printed and it is due to software problems. The output file says these things:

NA Method not applicable

NDM No Datcom method exist

In addition, tables 5.7 and 5.8 show the derivatives obtained from the Datcom simulations for each angle of attack.

As the Megastar which has an elevator, Shadow also has one, but in addition, it has another control device: ailerons. Table 5.9 shows the increments due to the deflection of the elevator and table 5.10 shows the yawing moment coefficient due to the deflection of the ailerons.

Fig. 5.5a, Fig. 5.5b and Fig. 5.6, show the graphics of the basic coefficients Cl and Cd versus the angle of attack and the Cd versus the Cl. After all the simulations have finished, the conclusion is that the critical angle of attack the Shadow is 17.4°. After this point, the values are not studies nor compared.

Table 5.7: Datcom derivatives coefficients for the Shadow (part 1)

Angles	CYB	CNB	CLB	CLQ	CMQ	CLR
-12°	-7,10E-03	1,25E-03	-7,10E-04	-5,97E-02	-1,62E-01	NDM
-8°	-7,10E-03	1,25E-03	-6,94E-04	-5,97E-02	-1,62E-01	NDM
-4°	-7,10E-03	1,25E-03	-6,71E-04	-5,97E-02	-1,62E-01	NDM
0°	-7,10E-03	1,25E-03	-6,46E-04	-5,97E-02	-1,62E-01	NDM
4°	-7,10E-03	1,25E-03	-6,22E-04	-5,97E-02	-1,62E-01	NDM
8°	-7,10E-03	1,25E-03	-5,94E-04	-5,97E-02	-1,62E-01	NDM
12°	-7,10E-03	1,25E-03	-5,46E-04	-5,97E-02	-1,62E-01	NDM
16°	-7,10E-03	1,25E-03	-4,69E-04	-5,97E-02	-1,62E-01	NDM
18°	-7,10E-03	1,25E-03	-4,11E-04	-5,97E-02	-1,62E-01	NDM
20°	-7,10E-03	1,25E-03	-3,05E-04	-5,97E-02	-1,62E-01	NDM

Table 5.8: Datcom derivatives coefficients for the Shadow (part 2)

Angles	CLAD	CMAD	CLP	CYP	CNP	CNR
-12°	1,37E-02	-3,64E-02	-9,52E-03	1,80E-04	1,30E-03	-9,12E-04
-8°	1,36E-02	-3,62E-02	-8,93E-03	-3,26E-05	6,61E-04	-8,77E-04
-4°	1,38E-02	-3,66E-02	-8,69E-03	-2,14E-04	5,05E-05	-8,91E-04
0°	1,38E-02	-3,67E-02	-9,13E-03	-3,96E-04	-5,69E-04	-9,47E-04
4°	1,35E-02	-3,59E-02	-9,74E-03	-6,07E-04	-1,23E-03	-1,06E-03
8°	1,35E-02	-3,58E-02	-9,10E-03	-8,41E-04	-1,95E-03	-1,22E-03
12°	9,88E-03	-2,63E-02	-6,45E-03	-1,01E-03	-2,63E-03	-1,40E-03
16°	3,04E-03	-8,07E-03	-1,23E-03	-1,06E-03	-3,16E-03	-1,52E-03
18°	-3,56E-03	9,45E-03	6,88E-03	-1,35E-03	-3,22E-03	-1,50E-03
20°	-8,03E-03	2,13E-02	1,97E-02	-1,32E-04	-4,32E-03	-1,33E-03

Table 5.9: Increments due to the deflection of the elevator in the Shadow

Delta	D(CL)	D(CM)	D(CL MAX)	D(CD MIN)
-8°	-0,039	0,0966	0,033	0,00185
0°	0	-0,0001	0	0
17°	0,075	-0,1847	0,062	0,00527

Table 5.10: Cn due to the deflection of the ailerons in the Shadow

	DeltaL - DeltaR		
Angles	**-28°**	**0°**	**54°**
-12°	-5,70E-03	0,00E+00	7,48E-03
-8°	-2,74E-03	0,00E+00	3,59E-03
-4°	4,11E-05	0,00E+00	-5,40E-05
0°	2,86E-03	0,00E+00	-3,75E-03
4°	5,91E-03	0,00E+00	-7,76E-03
8°	9,11E-03	0,00E+00	-1,20E-02
12°	1,17E-02	0,00E+00	-1,54E-02
16°	1,32E-02	0,00E+00	-1,73E-02
18°	1,31E-02	0,00E+00	-1,72E-02
20°	1,09E-02	0,00E+00	-1,43E-02

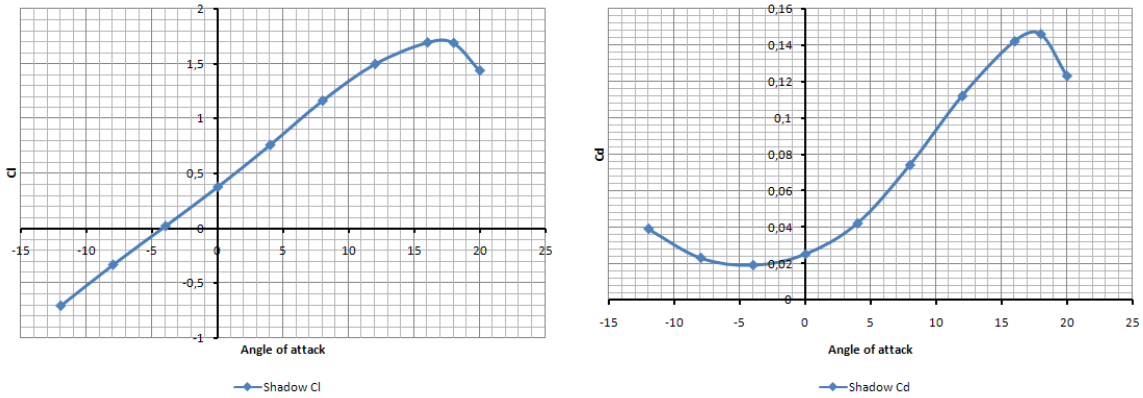

a) b)

Figure 5.5: a) Cl values from table 5.6 versus angle of attack. b) Cd values from table 5.6 versus angle of attack.

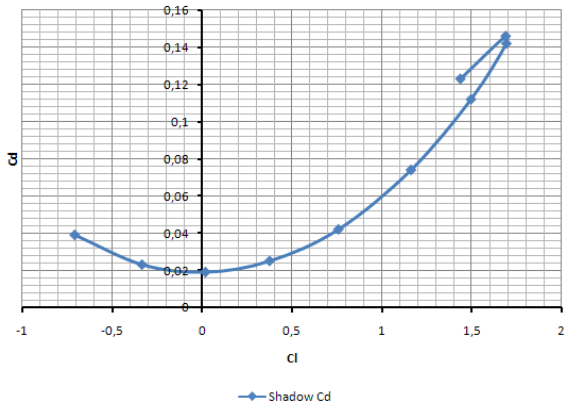

Figure 5.6: Cd values from table 5.6 versus Cl values of the same table

CHAPTER 6. COMPARISONS

This chapter will compare the different results obtained with Fluent and Datcom. The aerodynamic data obtained with Fluent is more accurate than the obtained with Datcom due to the way to obtain them, but the stability and control results obtained with Datcom are the only one because Fluent do not have the options to obtain them. Then, the results compared below will be the Cl and Cd data obtained with the two softwares.

6.1. Megastar

The Table. 6.1 shows the absolute error and relative error committed in the Cl and Cd results. The error arises in the last angles of attack because with Fluent, the stall condition starts later than with Datcom. The stall condition in Fluent starts at the angle of attack of 22° and 21° with Datcom. This significant difference could be due to the geometry approximation done with Datcom.

Table 6.1: Absolute and relative error of the results with Fluent and Datcom of the UAV Megastar

Angles	**Cl Absolute error**	**Cd Absolute error**	**Cl Relative error (%)**	**Cd Relative error (%)**
-12°	0,1050	0,0017	11,69	2,10
-8°	0,0295	0,0069	5,01	13,91
-4°	0,0031	0,0102	1,18	28,98
0°	0,0028	0,0107	4,24	33,79
4°	0,0214	0,0078	5,39	20,03
8°	0,0716	0,0008	9,88	1,30
12°	0,1725	0,0130	16,94	14,11
16°	0,2174	0,0067	16,95	4,40
20°	0,1240	0,0625	7,92	23,54
21°	0,0766	0,0943	4,70	30,99
22°	0,0177	0,1362	1,05	39,69
23°	0,0689	0,1658	4,10	44,96
24°	0,4376	0,2403	25,54	60,03
25°	0,8050	0,2969	47,78	70,71
26°	1,0962	0,3273	68,37	76,78

The Fig. 6.1a shows the Cl calculated with Fluent and Datcom. Althought the values differs in the high angles of attack, the maximum value of Cl is almost the same (≈1,707 with Datcom and ≈1,7136 with Fluent). This resemblance assures us that the simulations and their results are correct.

The Fig. 6.1b shows the Cd calculated with Fluent and Datcom. As shown in Table. 6.1 the values differ with high angles of attack. The values of datcom decline suddenly after entering in the stall condition. This could be due to the incapacity of Datcom to calcule the coefficients in the stall conditions due to the vortex generated. These vortexs could be

observed with the visualitation options of Fluent.

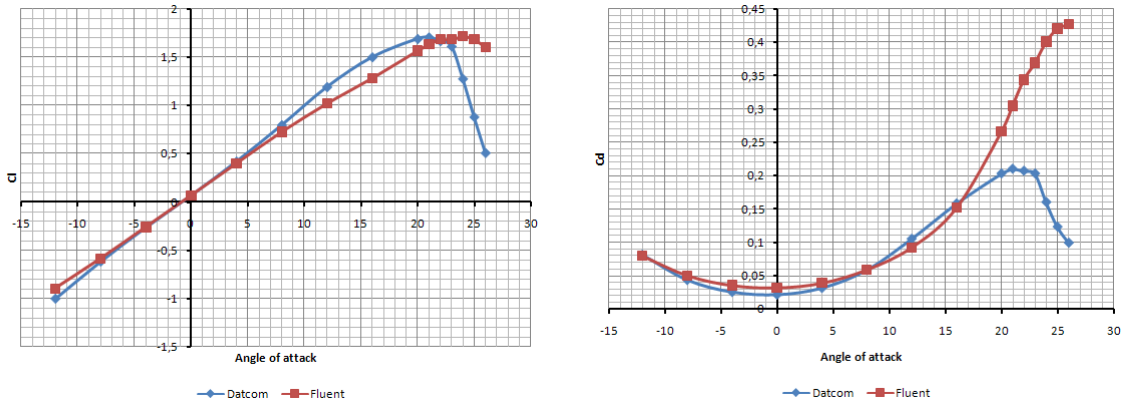

a) b)

Figure 6.1: a) Cl versus angle of attack obtained with Fluent and Datcom. b) Cd versus angle of attack obtained with Fluent and Datcom.

6.2. Shadow

The Table. 6.2 shows the absolute error and relative error committed in the Cl and Cd results. The error arises in the last angles of attack because with Fluent, the stall condition starts later than with Datcom. The stall condition in Fluent starts at the angle of attack of 23° and 17° with Datcom. This big difference is due to two factors, the geometry approximation done with Datcom (this model is more complex than the UAV Megastar), and the inhability to twist the outer angle of the wing with Datcom.

The twist of the outer angle of the wing is shown in a real image in Fig. 6.2. This angle is a negative angle that allows the UAV to enter in the stall condition some degrees later because as long as the part of the wing near the body has entered in the stall condition, the outer part has not because it has a negative angle respect the horitzontal. Then, as the geometry implemented with Gambit (see 4.2.) allows to twist the wing the stall condition starts later than with Datcom. That's why the highest value of Cl obtained with Datcom is ≈1,7 and with Fluent is ≈2.

Figure 6.2: Angle on the outer side of the wing of the UAV Shadow

The Fig. 6.3a shows the Cl calculated with Fluent and Datcom. In Table. 6.2 is observed a high value of error commited at -4° that the Fig. 6.3a does not represent. This error may be committed due to the inhability of the software to obtain results near 0°. This could be a typical error that had to be studied in more detail.

Table 6.2: Absolute and relative error of the results with Fluent and Datcom of the UAV Shadow

Angles	Cl Absolute error	Cd Absolute error	Cl Relative error (%)	Cd Relative error (%)
-12°	0,0744	0,0606	9,49	60,82
-8°	0,0576	0,0331	14,70	59,01
-4°	0,0214	0,0196	882,50	50,81
0°	0,0099	0,0114	2,57	31,41
4°	0,0173	0,0049	2,23	10,48
8°	0,0115	0,0084	1,00	12,75
12°	0,0219	0,0173	1,49	18,27
16°	-	-	-	-
18°	0,0133	0,0008	0,78	0,57
20°	0,4555	0,1181	24,06	48,99
22°	-	-	-	-
23°	-	-	-	-
24°	-	-	-	-
25°	-	-	-	-
26°	-	-	-	-
27°	-	-	-	-

The Fig. 6.3b shows the Cd calculated with Fluent and Datcom. As shown in Table. 6.2 the values differ with high angles of attack. There are not so many values after entering in the stall condition because the inutility of these values.

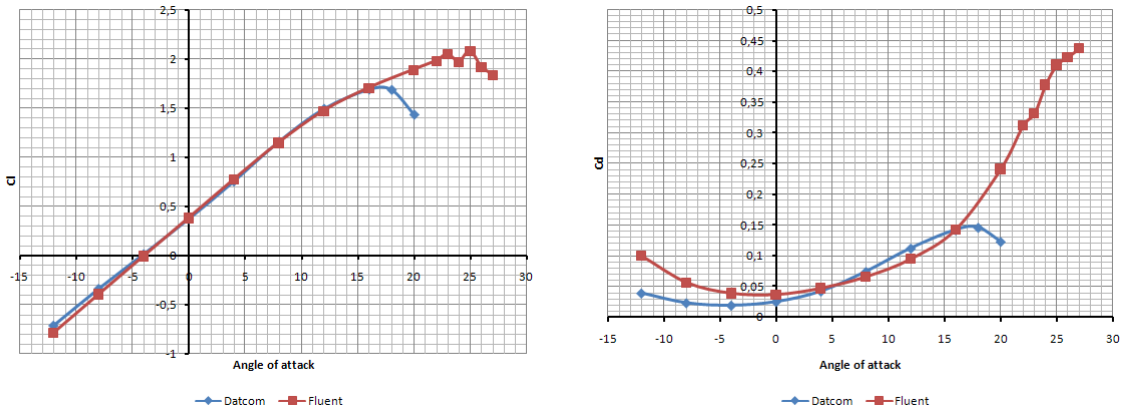

a) b)

Figure 6.3: a) Cl versus angle of attack obtained with Fluent and Datcom. b) Cd versus angle of attack obtained with Fluent and Datcom.

CONCLUSIONS

The objective of this work has been the computation of the aerodynamic coefficients corresponding to two aircrafts in order to calibrate the equations of stability and control needed for the programming of their autopilot. To obtain these coefficients, two softwares have mainly been used: Fluent and Datcom. Fluent is a software based on computational fluid dynamics and Datcom is a program which calculates the aerodynamic coefficients of an specific aircraft. The necessity to use both of them relays in the confidence to obtain as much coefficients as possible and also in the validation of the results comparing the values obtained with both softwares. The measurements of the geometries and their modelling into a design software have been the previous steps to the simulation of the aircrafts. Then, they have been simulated in many situations such as diverse angles of attack to take the more realistic values as possible.

Firstly, it is important to remark that this project is a continuation of others that have been done before. In previous projects,similar simulations were done, where aerodynamic parameters for the same vehicles were also analysed but only by using one of the softwares. This project is a first step to introduce new software and new aircraft modelling for future students and projects.

Moreover, the results obtained with Fluent and Datcom are similar, with differences for the lift coefficient around 5 to 10 per cent. These small differences are due to the different way of introducing the magnitude of the aircrafts in the two softwares. Fluent provides more efficient and realistic values than Datcom, but it only prints the drag and the lift coefficient, in addition to other physical magnitudes such as pressure or velocity. On the other hand, Datcom provides approximately values of lots of aerodynamic coefficients, which results very interesting due to its facility and faster calculation. For all these reasons, is very interesting to simulate any aircraft through these two useful softwares so one of the objectives of this project has been completed with success.

Finally, this project and its results could be a great help and a useful information tool for other students who continue with this matter. Further work may be done in order to gain accuracy with the results obtained. Datcom for example is a very complete and unusual software with lots of inputs which not all of them have been used in the simulations. It also provides an extensive output file that requires a determinant knowledge of each value. If further work is forseen, the simulations can be improved by adding more accurate geometries of the UAVs like: the landing gear or the tubes that connect the wing with the horizontal tail of the Shadow. Fluent, in contrast is a more well-known software, used in lots of applications but it also requires and extensive study of each case and of all the results, thus a wide understanding of them is essential to have good results. This results can be studied in more detail and the blades of the engine could be improved on the geometry by applying a pressure leap.

BIBLIOGRAPHY

[1] Free encyclopedia, http://en.wikipedia.org/wiki/Unmanned-aerial-vehicle

[2] Cox, T.H., Civil UAV capability assessment, NASA, December 2004.

[3] ICARUS Group, http://icarus.upc.edu/

[4] E.Pastor, J.Lopez, P.Royo., A Hardware/Software Architecture for UAV Payload and Mission Control, 25th Digital Avionics Systems Conference

[5] Integrated Dynamics, http://www.idaerospace.com/

[6] Theodore, A.T., Introduction to the aerodynamics of flight, Langley Research Center, NASA, Washington, D.C. 1975.

[7] Anderson, J.D., Fundamentals of aerodynamics / John D. Anderson, Boston, McGraw-Hill 2006.

[8] Stability and control information, http://selair.selkirk.bc.ca/aerodynamics1/Stability/default.htm

[9] Uy-Loi, Li, Stability and control of flight vehicle, Department of aeronautics and astronautics, University of Washington, Seattle 1997.

[10] Sci-tech encyclopedia, http://www.answers.com/topic/autopilot?cat=technology

[11] Aerodynamic and Aircraft Design Software, http://www.aoe.vt.edu/∼mason/Mason_f/MRsoft.html

[12] GAMBIT: Computational Fluid Dynamics (CFD) Preprocessor from Fluent, http://www.fluent.com/software/gambit/index.htm.

[13] FLUENT: Robust, Reliable, Comprehensive CFD Software, http://www.fluent.com/software/fluent/index.htm.

[14] VV.AA., The USAF stability and control Datcom, St. Louis division, McDonnell Douglas Astronautics Company, St. Louis 1979.

[15] Holi Cows, inc, http://www.holycows.net/datcom/

[16] PABLO Web page,http://www.nada.kth.se/∼chris/pablo/pablo.html

[17] XFOIL Subsonic Airfoil Development System, http://web.mit.edu/drela/Public/web/xfoil/

[18] Abbott, I.H., Theory of wing sections including a summary of airfoil data by Ira H. Abbott and Albert E. von Doenhoff, New York, Dover cop. 1959.

[19] NACA 4 Digits Series, http://www.pagendarm.de/trapp/programming/java/profiles/NACA4.html

[20] Avila, S.P., Estudi Aerodinàmic (CFD) d'un UAV, EPSC, 2006.

[21] UAV Navigation, http://www.uavnavigation.com/

[22] Anderson, J.D., Computational Fluid Dynamics, New York, Dover cop.

APÈNDIXS

APPENDIX A. UAV MODELS

In chronological order, ones of the most relevant UAV in the history are:

- Gyrodyne (QH-501960)
- RQ-2 Pioneer (1986)
- MQ- 1 Predator (1995)
- RQ-4 Global (Hawk2001)
- NASA Helios (2001)
- Boeing x-45 (2002)

A.1. Gyrodyne QH-50

The QH-50, better known as the DASH (Drone Anti-Submarine Helicopter), was a small, drone helicopter built by Gyrodyne for use as a long-range anti-submarine weapon of the US Navy on ships that would otherwise be too small to operate a full-sized helicopter. It remained in production until 1969. Several are still used today for various land-based roles. Its General characteristics are:

Length: 3.9 m.

Wingspan: -

Height: 3 m.

Empty weight: 537 kg.

Loaded weight: 991 kg

MTOW: 1.046 kg.

Powerplant: 190 kW.

Maximum speed: 148 km/h.

Range: 132 km.

Figure A.1: Gyrodyne QH-50. Source: [1]

A.2. RQ-2 Pioneer

Developed jointly by AAI Corporation and Israel Aircraft Industries, the RQ-2 has served with United States Navy, Marine, and Army units. Initially deployed aboard battleships to provide gunnery spotting, its mission evolved into reconnaissance and surveillance, primarily for amphibious forces. The ”R” is the Department of Defence designation for reconnaissance; ”Q” means unmanned aircraft system. The ”2” refers to it being the second of a series of purpose-built unmanned reconnaissance aircraft systems. Its General characteristics are:

Length: 4.3 m.

Wingspan: 5.2 m.

Height: 1 m.

Loaded Weight: 178 kg.

MTOW: 205 kg.

Powerplant: 19.4 kW.

Speed: 120-200 Km/h.

Range: 185 km.

Figure A.2: RQ-2 Pioneer. Source: [1]

A.3. MQ-1 Predator

The MQ-1 is an unmanned aerial vehicle which the U.S. Air Force describes as a MALE (medium-altitude, long-endurance) UAV system. It can serve in a reconnaissance role, and it can also be armed and can carry and use two missiles. The aircraft has been in use since 1995, and has been in combat over Afghanistan, Bosnia, Kosovo, Iraq, and Yemen. The fully UAS consists of four MQ-1, a ground control station, a primary satellite link communication suite and 55 persons. Its General characteristics are:

Length: 8.22 m.

Wingspan: 14.8 m.

Height: 2.1 m.

Loaded Weight: 512 kg.

MTOW: 1000 kg.

Powerplant: 75 kW.

Speed: 220 Km/h.

Range: 731 km.

Figure A.3: MQ-1 Predator. Source: [1]

A.4. RQ-4 Global Hawk

The Northrop Grumman RQ-4 is an unmanned aerial vehicle used by the US Air Force as a surveillance aircraft. In the US Air Force classification, this vehicle is a HALE UAV. It is the first UAV to be certified by the FAA to file its own flight plans and use civilian air corridors in the United States with no advance notice. Its General characteristics are:

Length: 13.5 m.

Wingspan: 35.5 m.

Height: 4.6 m.

Maximum Loaded Weight: 10.4 kg.

Thrust: 31.4 kN.

Speed: 650 Km/h at cruise.

Endurance: 34 hours.

Figure A.4: RQ-4 Global Hawk. Source: [1]

A.5. NASA Helios

In contrast with all the others UAV models, this one, is a civil UAV designed by the NASA. Helios was a solar and fuel cell system powered unmanned aircraft. Its significant goals were to reach an altitude near 30 km with a small payload on a single-day flight and flight for forty hours with at least fourteen of those hours above 15 Km. Helios was a forerunner of what some call artificial ”atmospheric satellites”. NASA claimed such atmospheric satellites might someday replace conventional artificial satellites. Its General characteristics are:

Length: 3.65 m.

Wingspan: 75.3 m.

Empty Weight: 600 kg.

Gross Weight: 910 kg.

Thrust: 31.4 kN.

Airspeed: 30-43 Km/h at low altitude

Endurance: With solar power, limited to daylight hours plus up to five hours of flight after dark on storage batteries. When equipped with a supplemental electrical energy system for nighttimes flight, from several days to several months.

Figure A.5: NASA Helios. Source: [1]

A.6. Boeing x-45

The Boeing X-45 Unmanned Combat Air Vehicle (UCAV) is a concept demonstrator for a next generation of completely autonomous fighter aircraft, developed by Boeing’s Phantom Works The X-45C is an unmanned, autonomous combat air vehicle that flies high-risk operational missions and delivers precision weapons on target. Controlled via either line-of-sight or satellite communications, the X-45C is highly adaptable to changing battle conditions and can provide electronic attack, reconnaissance, surveillance and intelligence gathering as well as engage in deep strikes to complement manned fighter and bomber forces. Its General characteristics are:

Length: 8.08 m.

Wingspan: 10.3 m.

Height: 3 m.

Empty Weight: 3630 kg.

Gross Weight: 5528 kg.

Speed: Subsonic.

Range: 600 Km.

Figure A.6: Boeing x-45. Source: [1]

APPENDIX B. SHADOW UAV AUTOPILOT

The autopilot used in the Shadow, is an autopilot of UAV Navigation [21], a privately owned company specialized in the design of flight control system for unmanned and manned aircraft.

It uses the AP04, a solution for both fixed and rotary wing UAVs. It is a fully integrated autopilot with manual override, radio link, and payload control capabilities.

The AP04 is used on UAVs ranging from micro-UAVs of less than 1 m. wingspan to medium UAVs of 4 m. wingspan, both fixed wing and helicopters. It is currently operating on electric, piston, and jet aircraft.

The AP04 is capable of fully automatic takeoff, hovering flight plan following, and landing. It can configure the aircraft for each stage of the flight, adapting flaps, or locking nose parachute or perform takeoff and land on standard runways.

Its integrated radio link allows data communication ranges in excess of 60 miles. Once a flight plan is loaded, no ground communications are needed. This extends the range of operation beyond radio reach. More characteristics are shown in Fig. B.1

FLIGHT CONTROL	
Fully automatic, multi-waypoint, 3D flight-plan following.	
Axis	3 (roll, pitch, yaw)
Auto throttle	Yes
Auto takeoff & landing	Yes
PAYLOAD MANAGEMENT	
Servo or I/O lines	16
Gyro-stabilization	Yes
Flare/parachute	Auto or manual firing
COMMUNICATIONS	
Baud rate	115.2 Kb/s (full duplex)
Range	100Km
Frequency	902-928MHz (1.3GHz option)
Method	Freq. hoping spread spectr.
Simult. multiple UAVs	Yes
I/O	
I/O lines	16
PWM rate	50Hz or 200Hz
PWM signal	1ms to 2ms high, 1us steps
RS232 ports baud rate	4.8K, 9.6K, 19.2K, 38.4K
REDUNDANCY & SAFETY	
Redundant processors	2
Online sensor diagnostics	Yes
Sensor failure tolerance	All single, several multiple

ADS	
Airspeed	0 to 300Kt
Altimeter	0 to 20,000ft
AHRS	
Accelerometer	3 axis
Max. acceleration	10G (vertical)
Angular rate sensors	3 axis
Max. angular rate	300°/s
Magnetometer	3 axis
Mag. attitude compensation	Yes
GPS	
Channels	12
Differential	Yes
ELECTRICAL	
Supply (unregulated)	7V to 14V
Current consumption	400mA
MECHANICAL/ENVIRONMENTAL	
Size (mm, H x W x L)	59.7 x 68.0 x 74.0
Weight	300gr
System connector	MS3112E-16-26P
Pressure connectors diameter	3.0mm
Radio link RF connector	SMA female
GPS RF connector	SMA female
Temperature range	-40°C to +85°C
Mounting screws	M4

Figure B.1: Characteristics of the autopilot. Source: [21]

APPENDIX C. GOVERNING EQUATIONS OF AERODYNAMICS

C.1. Fundamental physical principles

The fundamental governing equations of fluid dynamics [22], the continuity, momentum, and energy equations are the mathematical statements of three fundamental physical principles upon which all of fluid dynamics is based:

- Mass is conserved.
- Newton's second law $F = ma$.
- Energy is conserved.

These physical principles are applied to a model of the flow; in turn, this application results in equations which are mathematical statements of the particular physical principles involved. Each different model of the flow directly produces a different mathematical statement of the governing equations, some in conservation form and others in nonconservation form.

C.2. Models of the flow

In order to obtain the basic equations of fluid motion the appropriate fundamental physical principles from the law of physics have to be chosen to apply these physical principles to a suitable model of the flow and extract the mathematical equations which embody such physical principles. A definition for our suitable model is needed because if a solid body is moving translational to the flow the velocity of each part of the body is the same; on the other hand, if a fluid is in motion, the velocity may be different at each location in the fluid.

C.2.1. Finite control volume

This volume defines a control volume and a control surface defined as the closed surface which bounds the volume. The control volume may be fixed in space with the fluid moving through it as shown in Fig. C.2. Alternatively, the control volume may be moving with the fluid such that the same fluid particles are always inside it. The control volume is a reasonably large finite region of the flow. The fundamental physical principles are applied to the fluid inside the control volume and to the fluid crossing the control surface (if the control volume is fixed in space).

The equations obtained from the finite control volume moving with the fluid in integral or partial differential form are called the nonconservation form of the governing equations.

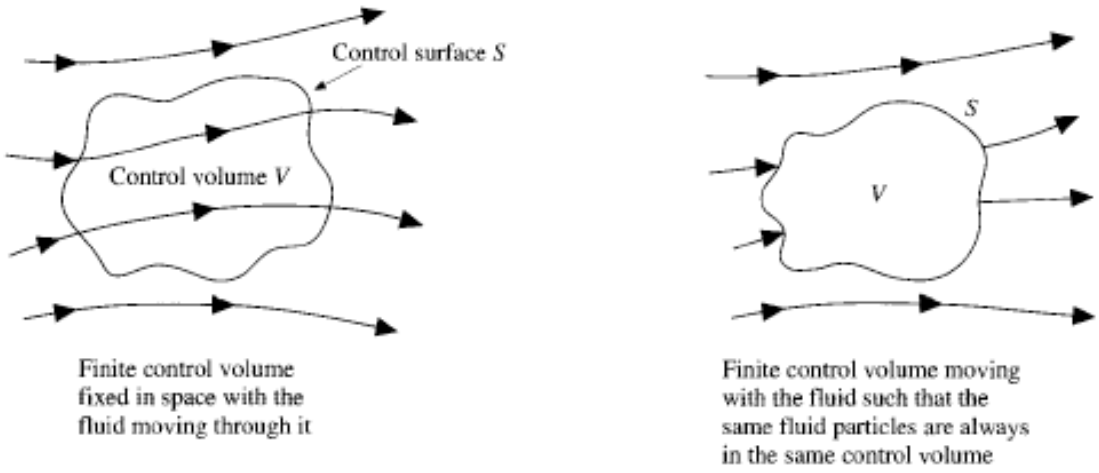

Figure C.1: Finite control volume. Source: [22]

C.2.2. Fixed infinitesimally small volume

Now, an infinitesimally small fluid element is observed in the flow with a differential volume. The fluid element is infinitesimal in the same sense as differential calculus. The fluid element may be fixed in space with the fluid moving through it as shown in Fig. C.2 or may be moving along a streamline with a velocity vector V equal to the flow velocity at each point. The fundamental physical principles are applied to just the infinitesimally small fluid element itself.

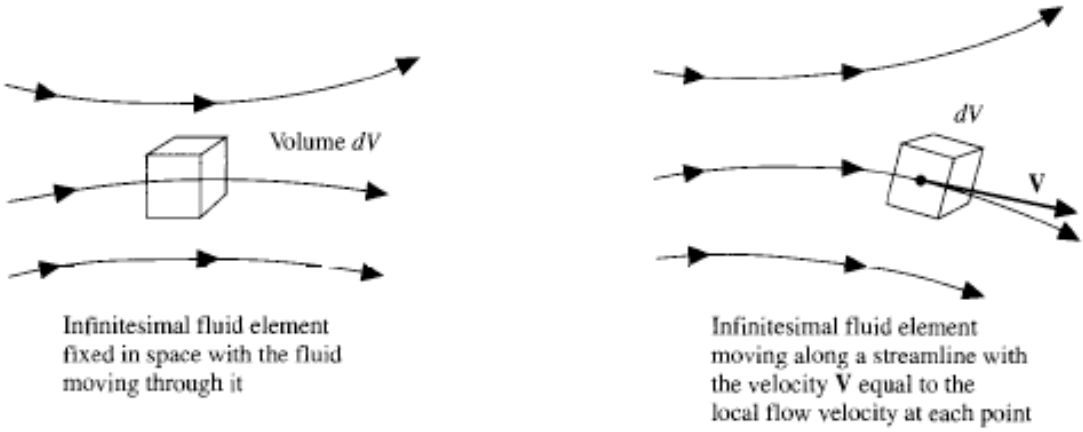

Figure C.2: Infinitesimal fluid element. Source: [22]

The particular partial differential equations obtained directly from the fluid element fixed in space are the conservation form of the equations. The partial differential equations obtained directly from the moving fluid element are called again the nonconservation form of the equations.

C.3. Governing Equations of fluid flow

C.3.1. Navier-Stokes Equations

The governing flow equation which results from the application of the physical principle that mass is conserved is called the continuity equation Eq. C.1

$$\frac{\partial \rho}{\partial t} + \nabla \cdot (\rho \mathbf{V}) = 0 \tag{C.1}$$

Momentum equation is obtained from the Newton's second law and can be referred to the different axis (x: Eq. C.2,y: Eq. C.3,z: Eq. C.4)

$$\frac{\partial \rho u}{\partial t} + \nabla \cdot (\rho u \mathbf{V}) = -\frac{\partial \rho}{\partial x} + \frac{\partial \rho \tau_{xx}}{\partial x} + \frac{\partial \rho \tau_{yx}}{\partial y} + \frac{\partial \rho \tau_{zx}}{\partial z} + \rho f_x \tag{C.2}$$

$$\frac{\partial \rho v}{\partial t} + \nabla \cdot (\rho v \mathbf{V}) = -\frac{\partial \rho}{\partial x} + \frac{\partial \rho \tau_{xy}}{\partial x} + \frac{\partial \rho \tau_{yy}}{\partial y} + \frac{\partial \rho \tau_{zy}}{\partial z} + \rho f_y \tag{C.3}$$

$$\frac{\partial \rho w}{\partial t} + \nabla \cdot (\rho w \mathbf{V}) = -\frac{\partial \rho}{\partial x} + \frac{\partial \rho \tau_{xz}}{\partial x} + \frac{\partial \rho \tau_{yz}}{\partial y} + \frac{\partial \rho \tau_{zz}}{\partial z} + \rho f_z \tag{C.4}$$

Energy equation Eq. C.5 is obtained from the physical principle that energy is conserved.

$$\frac{\partial}{\partial t}\left[\rho\left(e + \frac{V^2}{2}\right)\right] + \nabla \cdot \left[\rho\left(e + \frac{V^2}{2}\right)\mathbf{V}\right] = \rho \dot{q} - \frac{\partial (up)}{\partial x} - \frac{\partial (vp)}{\partial y} - \frac{\partial (wp)}{\partial z} + \rho \mathbf{f} \cdot \mathbf{V} \tag{C.5}$$

C.3.2. Equations suited for Computational Fluid Dynamics

Every governing equation has a divergence term on the left-hand side. These terms involve the divergence of the flux of some physical quantity such as mass flux, flux of x component of momentum or flux of total energy. Looking at the conservation forms, it is remarkable that they all have the same generic form of Eq. C.6.

$$\frac{\partial U}{\partial t} + \frac{\partial F}{\partial x} + \frac{\partial G}{\partial y} + \frac{\partial H}{\partial z} = J \tag{C.6}$$

Eq. C.6 can represent the entire system of governing equations in conservation form if U, F, G, H and J are interpreted as column vectors, given by Eqs. (3.7) to (3.11)

$$U = \left\{ \begin{array}{l} \rho \\ \rho u \\ \rho v \\ \rho w \\ \rho \left(e + \frac{V^2}{2} \right) \end{array} \right\} \tag{C.7}$$

$$F = \left\{ \begin{array}{l} \rho u \\ \rho u^2 + p - \tau_{xx} \\ \rho v u - \tau_{xy} \\ \rho w u - \tau_{xz} \\ \rho \left(e + \frac{V^2}{2} \right) u + p u - k \frac{\partial T}{\partial x} - u \tau_{xx} - v \tau_{xy} - w \tau_{xz} \end{array} \right\} \tag{C.8}$$

$$G = \left\{ \begin{array}{l} \rho v \\ \rho u v - \tau_{yx} \\ \rho v^2 + p - \tau_{yy} \\ \rho w u - \tau_{yz} \\ \rho \left(e + \frac{V^2}{2} \right) v + p v - k \frac{\partial T}{\partial y} - u \tau_{yx} - v \tau_{yy} - w \tau_{yz} \end{array} \right\} \tag{C.9}$$

$$H = \left\{ \begin{array}{l} \rho v \\ \rho u w - \tau_{zx} \\ \rho u w - \tau_{zy} \\ \rho w^2 + p - \tau_{zz} \\ \rho \left(e + \frac{V^2}{2} \right) w + p w - k \frac{\partial T}{\partial z} - u \tau_{zx} - v \tau_{zy} - w \tau_{zz} \end{array} \right\} \tag{C.10}$$

$$J = \left\{ \begin{array}{l} 0 \\ \rho f_x \\ \rho f_y \\ \rho f_z \\ \rho \left(u f_x + v f_y + w f_z \right) + \rho \dot{q} \end{array} \right\} \tag{C.11}$$

Note that the first elements of the U, F, G, H and J vectors, when added together via Eq. C.6, reproduce the continuity equation. Columns vectors F, G and H are called the flux terms and J represents a source term (which is zero if body forces and volumetric heating are negligible.) The column vector U is called the solution vector because the elements in U are the dependent variables which are usually obtained numerically in steps of time. If the solution is obtained throughout a marching solution based on space marching F, G and H is the solution vector depending on the direction of the flow computed in the simulation.

APPENDIX D. COMPUTATIONAL FLUID DYNAMICS

D.1. What is computational fluid dynamics?

Computational fluid dynamics [22], called with the extended acronym CFD is considered the art of replacing the integrals of the partial derivatives in the governing equations (see C) of aerodynamics with discretized algebraic forms, which in turn are solved to obtain numbers for the flow field values at discrete points in time and /or space. All these values are generally also showed with color maps as in Fig. D.1.

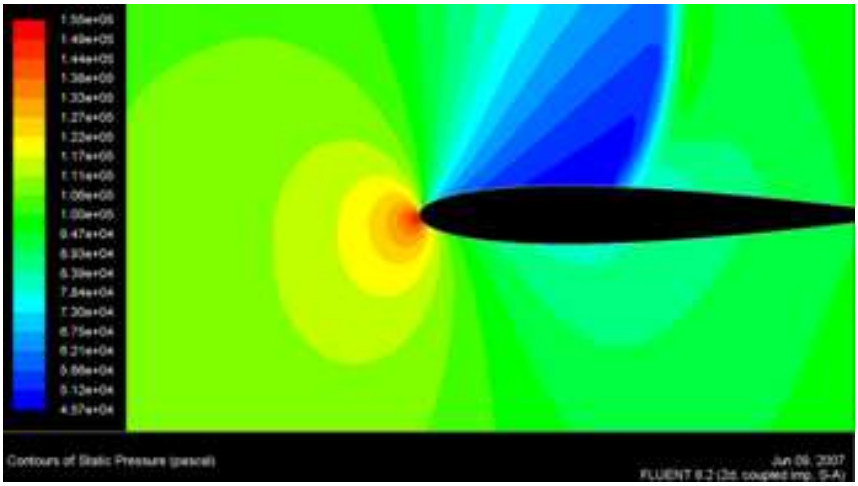

Figure D.1: Contours of static pressure of a NACA0012 airfoil simulated with Fluent

CFD solutions generally require the repetitive manipulation of many thousands, even millions, of numbers, a task that is humanly impossible without the aid of a computer. Therefore, advances in CFD, and its applications to problems of more and more detail and sophistication, are intimately related to advances in computer hardware, particularly in regard to storage and execution speed.

D.2. Discretitazion techniques

Discretization is the process by which a closed-form mathematical expression, such as a function or a differential or integral Eq. involving functions, all of which are viewed as having an infinite continuum of values throughout some domain, is approximated by analogous expressions which prescribe values at only a finite number of discrete points or volumes in the domain.

D.2.1. Finite difference

The essence of finite-difference solutions in CFD is to use the difference quotients; this need comes because discretizations of partial differential Equations are required to run a computer simulation. Most common finite difference representations of derivatives are based on Taylor's series expansions. Difference expressions for derivatives can be obtained with a forward, rearward or central difference. Higher order accurate difference quotients makes the calculation more exact and with less truncation error but with more time in each step of the calculation.

Eq. D.1 is an example of first order forward difference.

$$\left(\frac{\partial u}{\partial x}\right)_{i,j} = \frac{u_{i+1,j} + u_{i,j}}{\Delta x} \tag{D.1}$$

Eq. D.2 is an example of first order central difference.

$$\left(\frac{\partial u}{\partial x}\right)_{i,j} = \frac{u_{i+1,j} - u_{i-1,j}}{\Delta x} \tag{D.2}$$

Eq. D.3 is an example of second order central difference.

$$\left(\frac{\partial^2 u}{\partial x^2}\right)_{i,j} = \frac{u_{i+1,j} - 2u_{i,j} + u_{i-1,j}}{(\Delta x)^2} \tag{D.3}$$

Eq. D.4 is an example of how to implement these finite differences in a partial difference Eq..

$$\frac{\partial T}{\partial t} = \alpha \frac{\partial^2 y}{\partial x^2} \rightarrow \frac{T_{i+1,j} + T_{i,j}}{\Delta t} = \alpha \frac{T_{i+1,j} - 2T_{i,j} + T_{i-1,j}}{(\Delta x)^2} \tag{D.4}$$

D.2.2. Explicit and implicit approaches

In an explicit approach each difference equations contains only one unknown and therefore can be solved explicitly for this unknown in a straightforward manner. The advantage of this approach is the simplicity to set up and program whereas stability is harder to achieve. In some cases Δt has to be very small to maintain stability and this solution will result in long computer running times. The Eq. D.5 allows for an immediate solution of T_i^{n+1} from the known properties at time level n. It is a single equation with a single unknown.

$$T_i^{n+1} = T_i^n + \alpha \frac{\Delta t}{(\Delta x)^2} \left(T_{i+1}^n - 2T_i^n + T_{i-1}^n\right) \tag{D.5}$$

An implicit approach is one where the unknowns must be obtained by means of a simultaneous solution of the difference Equations applied at all the grid points at a given time level. Because of this need to solve large systems of simultaneous algebraic Equations, implicit methods are usually involved with the manipulations of large matrices. This point complicates the set up and the programming codes. Furthermore the computer time per time step will be longer than in the explicit approach. On the other hand, stability can be maintained over much larger values of Δt that will reduce computer time. The Eq. D.6 needs to be solved simultaneous at all the grid points because the right side contains the implicit solution of T.

$$\frac{(T_i^{n+1} - T_i^n)}{\Delta t} = \alpha \frac{\frac{1}{2}\left(T_{i+1}^{n+1} + T_{i+1}^n\right) + \frac{1}{2}\left(-2T_i^{n+1} - 2T_i^n\right) + \frac{1}{2}\left(T_{i-1}^{n+1} + T_{i-1}^n\right)}{(\Delta x)^2} \tag{D.6}$$

D.2.3. Stability analysis

As seen in the previous section t it is a factor to determine stability of a simulation. The stability of a calculation depends on the numerical errors that are generated throughout the course of a given calculation and it propagation from one marching step to the next. If this error is bigger in going from one step to the next, the calculation will become unstable; if the error does not grow and decreases, then the simulation usually has a stable behaviour.

There are two sources of this error. The difference between the exact analytical solution of the partial differential Eq. and the exact solution of the difference Eq. plus errors introduced by the numerical treatment of the boundary conditions are called the discretization errors. The numerical error introduced after a repetitive number of calculations in which the computer is constantly rounding the numbers to some numbers of decimals is called the round-off error.

Through an analysis called the von Neumann stability method it is possible to obtain a stability criterion synthesized in Eq. (4.7) where clearly shows that for a given Δx, the allowed value of Δt must be small enough to satisfy the Eq. D.7.

$$\frac{\alpha \Delta t}{(\Delta x)^2} \leq \frac{1}{2} \tag{D.7}$$

D.3. Computational fluid dynamics techniques

D.3.1. General ideas

Time marching means that the variable at all grid points at time level $n+1$ is calculated from the known values at time level n. When this calculation is finished you can continue with the same procedure used to calculate the variable at time $n+1$ to calculate the variable at the time $n+2$. This procedure is shown in Fig. D.2. This procedure assumes that

you know all the properties at time level *n* to calculate them at the next time level.

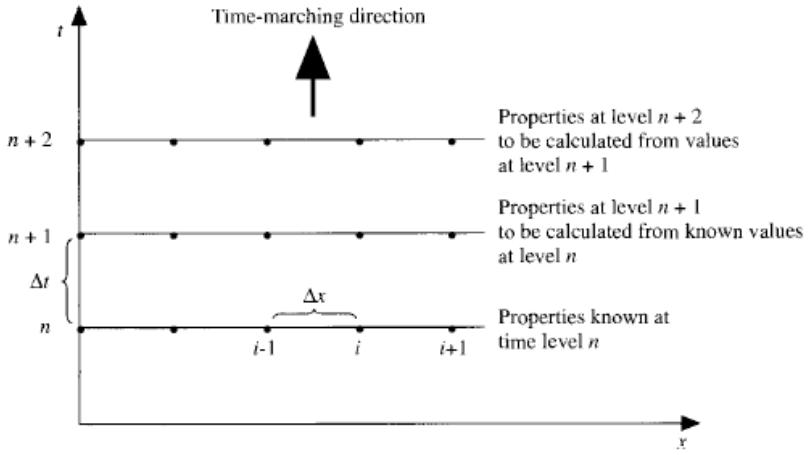

Figure D.2: Schematic grid for time marching. Source: [22]

Space marching means that the variable at the point j+1 is calculated from the known values at the point n. Assuming that the flow-field variables are known along the vertical line in the *xy* plane, this is the initial data line. Then a solution can be obtained, starting with the initial data line and marching in the *x* direction. It is the same procedure explained before in the time marching but with *x* steps. This procedure is shown in Fig. D.3.

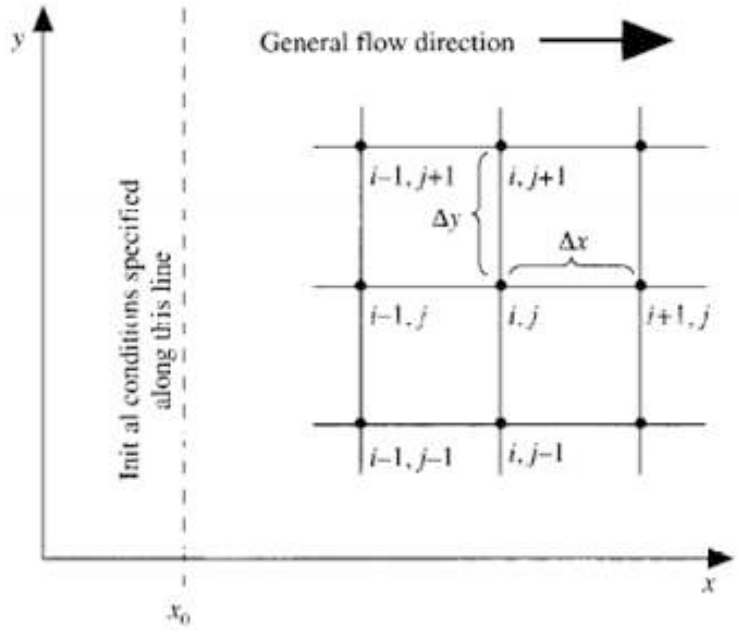

Figure D.3: Schematic grid for space marching. Source: [22]

D.3.2. Lax-Wendroff technique

The Lax-Wendroff technique is an explicit, finite-difference method particularly suited to marching solutions. In order to explain this method it is necessary to set up a numerical solution to continuity Eq. D.8 with no body forces and no volumetric addition.

$$\frac{\partial \rho}{\partial t} = -\left(\rho\frac{\partial u}{\partial x} + u\frac{\partial \rho}{\partial x} + \rho\frac{\partial v}{\partial y} + v\frac{\partial \rho}{\partial y}\right) \tag{D.8}$$

The next step implies employing Taylor series expansion in time as follows in Eq. D.9 up to second order. When employing Taylor series the flow field at time t is known and Eq. D.9gives the new flow field at time $t+\Delta t$.

$$\rho_{i,j}^{t+\Delta t} = \rho_{i,j}^{t} + \left(\frac{\partial \rho}{\partial t}\right)_{i,j}^{t}\Delta t + \left(\frac{\partial^2 \rho}{\partial t}\right)_{i,j}^{t^2}\frac{(\Delta t)^2}{2} + \cdots \tag{D.9}$$

Now it is time to discretize Eq.D.8 employing the method described in D.2.1. to determine the time derivatives used in Eq. D.9.The equation obtained is Eq. D.10. All quantities on the right side are known because the flow field at time t is known. This takes care of the second term on the right side of Eq. D.9, the third term is obtained in a similar fashion but requires more calculus.

$$\begin{aligned}\left(\frac{\partial \rho}{\partial t}\right)_{i,j}^{t} = -\Bigg(&\rho_{i,j}^{t}\frac{u_{i+1,j}^{t} - u_{i-1,j}^{t}}{2\Delta x} + u_{i,j}^{t}\frac{\rho_{i+1,j}^{t} - \rho_{i-1,j}^{t}}{2\Delta x} + \\ &+\rho_{i,j}^{t}\frac{v_{i,j+1}^{t} - v_{i,j-1}^{t}}{2\Delta y} + v_{i,j}^{t}\frac{\rho_{i,j+1}^{t} - \rho_{i,j-1}^{t}}{2\Delta y}\Bigg)\end{aligned} \tag{D.10}$$

In order to obtain all the new values of the properties at time $n+1$ the same procedure has to be done with the rest of the other flow-field variables applying it to the other governing equations.

D.3.3. Maccormack's technique

MacCormack's technique is a variant of the Lax-Wendroff approach but is much simpler in its application. The MacCormack method is also an explicit finite-difference technique which is second-order-accurate in both space and time. The same considerations as in Lax-Wendroff technique are assumed. In Maccormack's technique the flow field at time $t+\Delta t$ is obtained from Eq. D.11.

$$\rho_{i,j}^{t+\Delta t} = \rho_{i,j}^{t} + \left(\frac{\partial \rho}{\partial t}\right)_{av}\Delta t \tag{D.11}$$

The average time derivative $(\partial\rho/\partial t)_{av}$ is obtained from a predictor-corrector philosophy as follows. Predictor step consists to replace the spatial derivatives on the right-hand side with forward differences as in Eq. D.12.

$$\left(\frac{\partial\rho}{\partial t}\right)_{i,j}^{t} = -\left(\rho_{i,j}^{t}\frac{u_{i+1,j}^{t}-u_{i,j}^{t}}{\Delta x}+u_{i,j}^{t}\frac{\rho_{i+1,j}^{t}-\rho_{i,j}^{t}}{\Delta x}+\right.$$
$$\left.+\rho_{i,j}^{t}\frac{v_{i,j+1}^{t}-v_{i,j}^{t}}{\Delta y}+v_{i,j}^{t}\frac{\rho_{i,j+1}^{t}-\rho_{i,j-1}^{t}}{2\Delta y}\right) \tag{D.12}$$

All flow variables at time t are known values, and then throughout Eq. D.13 A predicted value is obtained from the first two terms of a Taylor series.

$$(\overline{\rho})_{i,j}^{t+\Delta t} = \rho_{i,j}^{t} + \left(\frac{\partial\rho}{\partial t}\right)_{i,j}^{t}\Delta t \tag{D.13}$$

In a similar fashion, predicted values for the other flow field variables are obtained. Corrector step consists to replace the spatial derivatives on the right-hand side with rearward differences as in Eq. D.14 using the predicted values calculated in the predictor step.

$$\left(\frac{\overline{\partial\rho}}{\partial t}\right)_{i,j}^{t+\Delta t} = -\left((\overline{\rho})_{i,j}^{t+\Delta t}\frac{(\overline{u})_{i,j}^{t+\Delta t}-(\overline{u})_{i-1,j}^{t+\Delta t}}{\Delta x}+(\overline{u})_{i,j}^{t+\Delta t}\frac{(\overline{\rho})_{i,j}^{t}-(\overline{\rho})_{i,j}^{t+\Delta t}}{\Delta x}+\right.$$
$$\left.+(\overline{\rho})_{i-1,j}^{t+\Delta t}\frac{(\overline{v})_{i,j}^{t+\Delta t}-(\overline{v})_{i,j-1}^{t+\Delta t}}{\Delta y}+(\overline{v})_{i,j}^{t+\Delta t}\frac{(\overline{\rho})_{i,j}^{t+\Delta t}-(\overline{\rho})_{i,j-1}^{t+\Delta t}}{2\Delta y}\right) \tag{D.14}$$

The average value of the time derivative of density which appears in Eq. D.11 is obtained from the arithmetic mean of $(\partial\rho/\partial t)_{i,j}^{t}$, obtained from Eq. D.12, and $\left(\overline{\partial\rho}/\partial t\right)_{i,j}^{t+\Delta t}$, obtained from Eq. D.14.

$$\left(\frac{\partial\rho}{\partial t}\right)_{av} = \frac{1}{2}\left[\left(\frac{\partial\rho}{\partial t}\right)_{i,j}^{t}+\left(\frac{\overline{\partial\rho}}{\partial t}\right)_{i,j}^{t+\Delta t}\right] \tag{D.15}$$

This allows us to obtained the final corrected value of the flow field variable at time $t+\Delta t$ from Eq. D.11. This sequence is repeated at all grid points and with all field flow variables.